POLITECNICO DI TORINO

Corso di Laurea Magistrale

Ingegneria Energetica e Nucleare

Tesi di Laurea Magistrale

Radioactive Dust Simulations with Monte Carlo

Relatore

Prof. Sandra Dulla

Dott. Alice Bonin (CEA Saclay)

Candidato

Matteo Zammataro

Dicembre 2019

List of Figures

List of Tables

1 Introduction

In the context of nuclear transition scenarios, radiation shielding assessments of fuel fabrication plants are carried on. The fuel is a mixture of uranium-plutonium oxide. In a fuel fabrication plant the oxide power is pressed in the pressing workplace to produce fuel pellets.

The radiation shielding study of the pressing workplace consists in calculating sources using DARWIN-PEPIN 2® evolution code and then in calculating the ambient dose equivalent rate with TRIPOLI-4® radiation transport code in several locations (in front of the mixing jar, in front of the pressing table, at the extremities). Current model of the pressing workplace does not take into account potential dust that is likely to appear and to deposit on some surfaces.

For this reason, a modeling work of radioactive dust and parametrical analysis of its possible contributes to the dose equivalent rate is presented in this thesis. In particular, importance will be given to the differences between the microscale and macroscale modeling of the radioactive source, in order to highlight the behavior of disordered media in this case of study.

1.1 Aim of the Thesis

The aim of the work is to provide a better radioprotection analysis of one of the crucial part of the fuel cycle: the pressing workplace [1]. Inside a glove box containing radioactive materials it is possible to find radioactive dust accumulated in some surfaces. To take into account the possible contribution on the dosimetry calculation in the glove box due to this radioactive dust, suitable models and calculation procedures must be designed.

In radiation protection calculations, dealing with dispersed or disordered media such a distribution of radioactive dust in a big environment, the homogenization of such media is widely used. The question motivating the present work is whether a homogenized system is sufficient to simulate properly this kind of problem, where substantially the radioactive source can be dispersed in the air, or well accumulated in a finite number of regions of the system.

In fact, different kind of dust distribution could be found in a glove box, from the simple deposition on a plane surface with a low accumulation density to the formation of dense aggregates in the corners of the box. To better understand if a homogeneous model is capable to take into account different shapes, concentrations and distributions of the radiation source, there is the need to find a proper way to simulate each one of these conditions.

The fundamental point is, in fact, simulating in microscale really small objects to make a comparison in terms of transport properties with the homogenized models to understand if, case by case, the dose equivalent rate obtained with the homogeneous model is overestimated or underestimated.

Several models to simulate the radioactive dust in different configurations are here provided, taking advantage of the capability of the TRIPOLI-4® code to simulate radiation transport in stochastic geometries.

1.2 State of the Art

In the field of reactor physics it is really common to find both the homogeneous and stochastic models [2, 3]. In fact, while a stochastic geometry allows to study in deep some phenomena, like radiation transport in pebble-bed type reactors [4] or in corium scenarios [5], a model obtained with the averaging, or homogenization of the material properties can often be a good compromise between the accuracy of the results and the computational cost of the simulations.

In literature it is possible to find many examples of particle transport studies in disordered, or stochastic geometries. What emerges from these studies is the importance of the chord length distribution of the geometry. Intuitively this value, coupled with the mean free path of the particles, represents the quantity of objects that the particles "see" during a flight. If this number of objects is high enough, we can assume that we will not lose information using a homogenized system instead of a discrete one. Instead, if this number is small, importance must be given to the material composition of the medium traversed by the particle, and this can be done only by considering the material composition of the system as it is in the reality [6]. It is important to keep in mind the concept of atomic mix in order to easily understand in which situations it is possible to have more information using a microscale approach.

1.3 Nuclear Fuel Cycle

In the nuclear energy industry the nuclear fuel cycle plays a fundamental role. Different strategies are used in this field, and in general, we can classify the itineraries of the uranium from the mine to the reactor and then to the waste storage in two categories: open fuel cycle and closed fuel cycle. A schematic representation can be found in Figure 1.

The fundamental advantage of the closed cycle is that is possible to recover a consistent part of the fuel instead of using it just once and then storing it in a waste disposal. In fact, most of the nuclear fuel can be recycled, and sent again to the starting point of the loop. Doing this means reprocessing the fuel, in other words it means separating the plutonium and the high level wastes from the depleted uranium, and then mixing the recovered plutonium to other materials to obtain a Mixed Oxide Fuel (MOX).

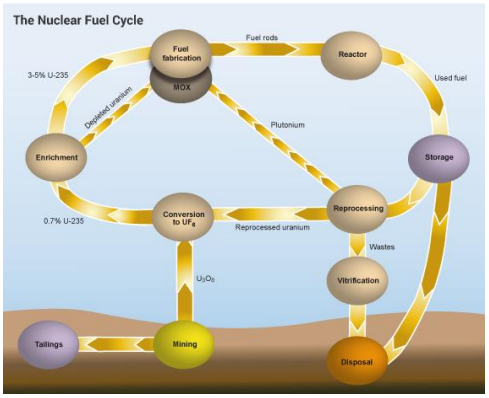

Figure 1: the nuclear fuel cycle. Image coming from: https://energyeducation.ca/encyclopedia/Nuclear_fuel_cycle.

1.3.1 Glove Box

The general context of this work concerns one part of the nuclear fuel cycle, in particular the production of fuel pellets [1] to be used in nuclear reactors. This falls in the field of fuel fabrication, and it is specifically the phase of fuel fabrication in which the nuclear fuel, initially pulverized, is pressed in small cylinders shape before being heated in an oven. The pressing process is performed with a set of machines, namely the Pressing Workplace. Most of the operations are here carried out by using automatic processes, but sometimes the intervention of an operator is required, for some maintenance operations or other very specific duties. For this reason the pressing workplace uses a glove box: a steel box with a single glass-made wall, with the possibility of inserting the hands in two gloves welded to the glass. A picture of a glove box is visible in Figure 2. This solution allows efficient human interventions with a protection against hazards, since the glove box is always completely sealed and the envelope, gloves also, provides a sufficiently good radiation shielding.

Figure 2: An operator weighting powder using a glove box in the CEA Cadarache research center. Image coming from the website: http://www.cea.fr/english/Pages/research-areas/nuclear-energy/nuclear-fuel.aspx?Type=Chapitre&numero=3.

1.4 Radiation Protection

Radiation protection is the science and practice of protecting people and the environment from the harmful effects of ionizing radiation. The International Atomic Energy Agency (IAEA) defines radiation protection as:
"The protection of people from harmful effects of exposure to ionizing radiation, and the means for achieving this".
It is an important topic not only in the field of nuclear energy, but also in industrial or in medical applications.

1.4.1 Radiation Protection Principles

According to the ICRP [7], the System of Radiological Protection is based on the following three principles:

1. Justification: the exposition to a radiation source must be taken into account only if the benefits coming from the exposition are sufficient to justify it.

2. Optimization of Protection: once the principle of justification is satisfied, the exposition must be carried out having the maximum protection reasonably obtainable. This means that the procedure must last less time possible, and the irradiation conditions must be as safe as possible for the people.
3. Dose Limitation: once the first two principles are satisfied, the quantity of absorbed energy from radiations must be limited to certain values fixed by law [7].

1.4.2 Radiation Protection for External Exposure

The radiation exposure can basically be internal or external. In the first case, the radioactive substance is inhaled or ingested by a person, and this leads to an exposition to particles of every kind, independently from their possibility to cross or not large portions of matter. In the second case, more appropriate to the case of study treated in this topic, the radiation source is outside the body, but the particles emitted interact with it. In this case the most dangerous particles are neurons and gamma photons, since they have the highest probability not to be absorbed before reaching the person. About the external radiation exposure, there are three ways to limit the dose to which people are exposed:

- Limiting Time: the energy deposed in living tissue depends linearly on the exposure time. So, to limit the absorbed radioactive dose equivalent, is fundamental to spend the less time possible in an exposure condition. With medical procedures, for example, this is directly correlated to the justification principle, according to what diagnostic or therapeutic procedures involving ionizing radiations could be used only if strictly necessary. In the industry environment, which involves the case of study of the topic, care must be given to the time passed in presence of radioactive sources, limiting it as much as possible;

- Distance. The amount of radiation exposure depends on the square of the distance from the source of radiation. Assuming a uniform probability density function for the angle of the emission of a source, and supposing it concentrated in its center, the probability for a point of coordinates r to be reached by a particle coming from r'can be written as follows:

$$P = \frac{1}{4\pi\lceil r - r'\rceil^2} \tag{1}$$

  So, the probability is inversely proportional to the square of the distance between the source and the point. That means that passing the double of the time in presence of a radioactive source but at a double distance, for example, implies the half of the absorbed radioactive dose.

- Shielding. Finally, if the source is too intensive and time or distance do not provide sufficient radiation protection, the shielding must be used. It consists in the creation of a barrier between the radioactive source and the environment, which can be made of different materials, depending on the situation. Radiation shielding can be studied using the Lambert-Beer's law [8]:

$$T = \frac{I}{I_0} = e^{-\int_0^s ds' \mu(s')} \quad (2)$$

where I, I_0 are respectively the radiation intensity before and after the shield, and $\mu(s)$ is the radiation attenuation coefficient at the position s. This coefficient depends on the material and on the particle who cross it. For example, for a shield composed by lead, the value of μ will be much greater for gamma photons than for neutrons.

1.4.3 Radiation Dosimetry

In Radiation Dosimetry, over considering physical quantities like the absorbed dose, the biological effectiveness of the radiation must be taken into account. The biological effect of the radiations is dependent on the type and on the energy of the radiation itself, and this is the reason why analyzing the simple absorbed energy is not sufficient to understand how much an exposition could be dangerous. The dose quantity representing the stochastic effects on the human body, like radiation induced cancer and genetic damage, is the dose equivalent.

In the international system of units, the unity of measure for the dose equivalent is the Sievert $[Sv]$. The ambient dose equivalent H (10), expressed in $[\mu Sv/h]$ is used in this work.

To enable consideration of stochastic health risk, calculations are performed to convert the physical quantity absorbed dose into equivalent dose, the details of which depend on the radiation type. For applications in radiation protection and dosimetry assessment, the International Commission on Radiological Protection (ICRP) and the International Commission on Radiation Units and Measurements (ICRU) have published recommendations and data on how to calculate equivalent dose from absorbed dose.

The purpose of the ICRP was having a kind of threshold, or a limit, under which the occurrence of stochastic health effects in kept below unacceptable levels and the deterministic effects, like Acute Radiation Syndrome, are completely avoided. The dose equivalent, being a quantity obtained by weighting the absorbed energy, can't be practically measured, thus it is a quantity that is calculated, with the aim of generating a list of values that can be correlated to observed health effects.

Table 1: Quality factor W_R according to the type and energy of the radiation. Data coming from the website https://en.wikipedia.org/wiki/Sievert.

Radiation		W_R
X-rays, Gamma rays, Muons, β particles		1
Neutrons	< 1 MeV	$2.5 + 18.2 \cdot \exp[-\ln(E)]^2/6$
	1 MeV - 50 MeV	$5.0 + 17.0 \cdot exp[-ln(2 \cdot E)]^2/6$
	> 50 MeV	$2.5 + 3.25 \cdot exp[-ln(0.04 \cdot E)]^2/6$
Protons, Charged Pions		2
α Particles, Nuclear fission products, Heavy nuclei		20

Since different radiation types have different biological effects for the same deposited energy, a corrective radiation weighting factor, which depends on the radiation type and on the target tissue, is applied to convert the absorbed dose measured in Gray to determine the equivalent dose. The most common values of the weighting factor of each particle are shown in Table 1. The equivalent dose is calculated by multiplying the absorbed energy, averaged by mass over an organ or tissue of interest, by a radiation weighting factor appropriate to the type and energy of radiation. To obtain the equivalent dose for a mix of radiation types and energies, a sum is taken over all types of radiation energy dose.

2 Transport Model in Disordered Media

2.1 The Transport Equation

Radioprotection studies for nuclear dust in glove boxes requires to check the behavior of particles emitted by a radioactive material and traveling inside it. Basically it is called a Source Problem: a scenario of particle transport in which the aim is to check the particle flux coming from a radioactive source, instead of checking the eigenvalues for a criticality study.

Taken $\phi(\vec{r}, E, \vec{\Omega}, t) = vn(\vec{r}, E, \vec{\Omega}, t)$, where ϕ represents the particle flux and n the density of the phase space in 7 dimensions, the transport of neutral particles is described by the Boltzmann Linear Transport equation [9]:

$$\begin{aligned} &\frac{1}{v}\frac{\partial\phi(\vec{r}, E, \vec{\Omega}, t)}{\partial t} + \sum_a(\vec{r}, E)\phi(\vec{r}, E, \vec{\Omega}, t) + \Omega \cdot \nabla\phi(\vec{r}, E, \vec{\Omega}, t) \\ &= S(\vec{r}, E, \vec{\Omega}, t) + \oint d\vec{\Omega}' \int dE' \Sigma_s(\vec{r}, E')\phi(\vec{r}, E', \vec{\Omega}', t) f_s(\vec{r}, E' \Rightarrow E, \vec{\Omega}' \cdot \vec{\Omega}) \\ &+ \oint d\vec{\Omega}' \int dE' \Sigma_f(\vec{r}, E')\phi(\vec{r}, E', \vec{\Omega}', t)\nu(\vec{r}, E')\frac{1}{4\pi} X(\vec{r}, E', \vec{\Omega}', t) \end{aligned} \tag{3}$$

where:

- $\frac{1}{v}\frac{\partial\phi(\vec{r},E,\vec{\Omega},t)}{\partial t}$ represents the variation of the particle phase space density in the time,
- $-\sum_a(\vec{r}, E)\phi(\vec{r}, E, \vec{\Omega}, t)$ represents the particles lost due to the absorption,
- $\Omega \cdot \nabla\phi(\vec{r}, E, \vec{\Omega}, t)$ the geometrical leakage,
- $\oint d\vec{\Omega}' \int dE' \Sigma_s(\vec{r}, E')\phi(\vec{r}, E', \vec{\Omega}', t) f_s(\vec{r}, E' \Rightarrow E, \vec{\Omega}' \cdot \vec{\Omega})$ the particles scattered in,
- $S(\vec{r}, E, \vec{\Omega}, t)$ the particles emitted by a source and finally
- $\oint d\vec{\Omega}' \int dE' \Sigma_f(\vec{r}, E')\phi(\vec{r}, E', \vec{\Omega}', t)\nu(\vec{r}, E')\frac{1}{4\pi} X(\vec{r}, E', \vec{\Omega}', t)$ the particles generated by fission.

Rearranging the terms of the equation, putting together generations and losses, it is possible to write the equation in a more compact form:

$$\frac{1}{v}\frac{\partial\phi}{\partial t} + \hat{L}\phi = S + \hat{F}\phi \tag{4}$$

Where $\hat{L}$ *and* $\hat{F}$ are the losses and fission operators.

Since our case of study does not involve fissions or transients, the problem collapses into:

$$\hat{L}\phi = S \tag{5}$$

2.1.1 The Peierls Equation

The solution of transport problems can be obtained using the method of characteristics to get the Peierls Equation. In particular, this integral equation links directly the particle flux in a point with the particle emission in another one. The extended expression is [9]:

$$\phi(\vec{r},E,\vec{\Omega}) = \phi(\vec{r}-s\vec{\Omega},E,\vec{\Omega})exp\left[-\int_0^s ds'\,\Sigma(\vec{r}-s'\vec{\Omega},E)\right] + \int_0^s ds'\,Q(\vec{r}-s'\vec{\Omega},E,\vec{\Omega})exp\left[-\int_0^{s'} ds''\,\Sigma(\vec{r}-s''\vec{\Omega},E)\right] \tag{6}$$

In other terms, particles in $\vec{r}$ with energy E and direction $\vec{\Omega}$ are the particles in $\vec{r}-s\vec{\Omega}$ multiplied by their probability to survive traveling for a distance s plus what is produced between 0 and s multiplied also by the probability to survive. This probability is the negative exponential of a quantity called *optical path length*, for definition:

$$l_{op} = \left[\int_0^{s'} ds''\,\Sigma(\vec{r}-s''\vec{\Omega},E)\right] \tag{7}$$

So the probability to traverse a medium without interaction, for a single particle in the phase space, is: $P_{interaction} = \exp(-l_{op})$

In literature a lot of numerical methods [10] to solve this kind of problems are given. Moreover, in this specific topic a Monte Carlo approach will be used for this purpose.

2.1.2 Particle Transport in Disordered Media

Let us consider a scenario in which the geometry is neither homogeneous nor regularly shape, to study what happens as far as transport is concerned. In that case the material composition of the medium must be taken into account in every position $\vec{r}$ considered as no homogenization has been performed. Assuming that the system is composed of a set of states $A = \{n\}$, to each state n it is possible to associate a value for the cross sections and for the source term. Considering a single energy level for the sake of simplicity, we can define [6]:

$$\langle\phi(\vec{r},\Omega)\rangle = \int dnP(n)\phi^{(n)}(\vec{r},\Omega) \tag{8}$$

where $\langle\phi(\vec{r},\Omega)\rangle$ is the formal definition of the angular flux averaged on the ensemble $A = \{n\}$, $P(n)$ is the probability of observing the state n and $\phi^{(n)}$ is the solution of the Boltzmann equation for the single n state:

$$\begin{aligned}\Sigma_t^{(n)}(\vec{r})\phi^{(n)}(\vec{r},\vec{\Omega}) + \Omega\cdot\nabla\phi^{(n)}(\vec{r},\vec{\Omega}) &= S^{(n)}(\vec{r},E,\vec{\Omega},t)\\ &+ \oint d\vec{\Omega}'\Sigma_s^{(n)}(\vec{r})\phi^{(n)}(\vec{r},\vec{\Omega}')f_s^{(n)}(\vec{r},\vec{\Omega}'\to\vec{\Omega})\\ &+ \oint d\vec{\Omega}'\,\Sigma_t^{(n)}(\vec{r})\phi^{(n)}(\vec{r},\vec{\Omega}')\nu(\vec{r})\frac{1}{4\pi}X(\vec{r},\vec{\Omega}')\end{aligned} \tag{9}$$

Taking into account a stochastic binary mixture composed of two materials α and β, so a geometry composed these two materials randomly distributed in space with known statistical laws in a defined control volume, transport equation can be rewritten considering source and cross sections as random variables:

$$\begin{aligned}\left(\vec{\Omega}\cdot\nabla+\Sigma_{t,\alpha}(\vec{r})\right)\cdot\left(p_\alpha(\vec{r})\langle\phi_\alpha(\vec{r},\vec{\Omega})\rangle\right) &= p_\alpha(\vec{r})\int d\Omega'\Sigma_{s,\alpha}(\Omega'\to\Omega)\langle\phi_\alpha(\vec{r},\Omega')\rangle + p_\alpha(\vec{r})Q_\alpha(\vec{r},\vec{\Omega})\\ &+ U_{\alpha,\beta}(\vec{r},\vec{\Omega})\end{aligned} \tag{10}$$

Where P_α corresponds to the probability of finding material α at position $\vec{r}$, formally defined as $P_\alpha(\vec{r}) = \int_{X_\alpha(\vec{r})} P(n)\,dn$, $X_{\alpha,(\vec{r})} = \{n\,\epsilon\,A|n(\vec{r})=\alpha\}$, Q_α representing the emission in material α and $U_{\alpha,\beta}(\vec{r},\vec{\Omega})$ being a coupling term that represents the probability of going from state α to state β at position $\vec{r}$ with direction $\vec{\Omega}$.

2.1.3 Chord Length Influence

In literature [11] studies about the relation between the chord length distribution of a material and its transport properties can be found. The average chord length is defined as the mean distance that is possible to travel in a component of type n following a straight trajectory. In a stochastic geometry, naturally, the chord length will vary with respect to the starting and finish points of the imaginary straight line one wants to follow, so it is logic to consider chord length statistics, such as mean and probability density function. In general in a convex solid, non-reentrant body the average chord length can be expressed by the ratio [12]:

$$\bar{\Lambda}_S = \frac{4\cdot Volume_S}{Surface_S} \tag{11}$$

Where index S denotes a generic solid object having the properties required above. In case of a homogeneous and isotropic dispersion of spheres with monodispersed radiuses, that is to say a binary mixture with state α corresponding to the spheres and state β to the matrix, it is possible to calculate explicitly both the average chord lengths of α and β [6]:

$$\bar{\Lambda}_\alpha = \frac{4}{3}R_{sph} \tag{12}$$

$$\overline{\Lambda_\beta} = \left(\frac{1}{\xi} - 1\right) \cdot \frac{4}{3} R_{sph} \tag{13}$$

where ξ is the Packing Fraction of the geometry, defined as:

$$\xi = \frac{V_\alpha}{V_\alpha + V_\beta} \tag{14}$$

In the case of poly-dispersed radius spherical inclusions it must be considered also the radius distribution, thus the average chord length definition becomes:

$$\bar{\Lambda}_\alpha = \frac{4}{3} \cdot \frac{\int dR \cdot f(R) R^3}{\int dR \cdot f(R) R^2} \tag{15}$$

$$\overline{\Lambda_\beta} = \left(\frac{1}{\xi} - 1\right) \cdot \frac{4}{3} \cdot \frac{\int dR \cdot f(R) R^3}{\int dR \cdot f(R) R^2} \tag{16}$$

This can be a practical example of situation in which the transport equation in stochastic binary mixture is valid. In this case:

$$p_\alpha(\vec{r}) = \frac{\Lambda_\alpha(\vec{r}, \Omega)}{\Lambda_\alpha(\vec{r}, \Omega) + \Lambda_\beta(\vec{r}, \Omega)} \tag{17}$$

and the probability per unit length of crossing an interface going from material α to material β can be written as:

$$p_{\alpha,\beta}(\vec{r}, \Omega) = \frac{p_\alpha(\vec{r})}{\Lambda_\alpha(\vec{r}, \Omega)} \tag{18}$$

2.1.4 Mean Free Path in Stochastic Media

Because the cross sections strictly depend on the position, and the portion of space traveled in each material depends on the position and direction, the formulation of the mean free path for homogeneous media, that is to say [13]:

$$mfp = \frac{1}{\Sigma_t} \tag{19}$$

cannot be used anymore. In practice, the method used to calculate the mean free path in a stochastic geometry is the same method used in the Monte Carlo transport simulation (see section 2.2.3).

It is thus possible to think in terms of expected value: the probability to travel distance s in a given medium is given by the optical path length integral. In this case, this integral will be a function of the position and of the direction:

$$p(s|\vec{r},\Omega) = l_{op}(\vec{r},\Omega) = \left[\int_0^{s'} ds''\, \Sigma\left(\vec{r} - s''\vec{\Omega},\Omega\right)\right] \tag{20}$$

It is possible to calculate a differential of this probability, thus:

$$dp(s|\vec{r},\Omega) = \; dp(s + ds|\vec{r},\Omega) - dp(s|\vec{r},\Omega) \tag{21}$$

This represents the probability to travel a length whose value is in the interval $[s\,;\; s + ds]$, and can be defined as:

$$dp(s|\vec{r},\Omega) = \left|\frac{\partial l_{op}}{\partial s}\right| \cdot \partial s = \left[\int_0^{s'} ds''\, \Sigma\left(\vec{r} - s''\vec{\Omega},\Omega\right)\right] * \Sigma\left(\vec{r} - s''\vec{\Omega},\Omega\right) ds \tag{22}$$

Now it is possible to rewrite the expression of the mean free path of a stochastic geometry in terms of expected value $E(s)$:

$$mfp(\vec{r},\Omega) = E(s|\vec{r},\Omega) = \int_{-\infty}^{+\infty} dp(s|\vec{r},\Omega) \cdot s \tag{23}$$

2.1.5 Atomic Mix Limit

This last section about particle transport in stochastic media has the aim to highlight the relation between the average chord length of the geometry and the mean free paths. In fact, the ratio between these two values is in practice equal to the number of material chunks that the particle "sees" during a flight. Basically, this implies that a large ratio requires a microscale approach, since the position of the particle can influence a lot the transport properties and, on the other hand, if the ratio is very small the position of the particle is not very relevant in terms of transport, since the length of material traversed by the particle will be large enough to lose information on what happens in a single chunk. This last condition is called "Atomic Mix Regime", and it can be demonstrated also mathematically that in this situation the transport equation in disordered media collapses into the transport equation for a homogeneous medium which has properties obtained by averaging the n states on the whole control volume. So, the atomic mix limit can be defined, for the single n state, as [11]:

$$\Lambda_n \cdot \Sigma_{t,n} \ll 1 \tag{24}$$

Eq. (24) is therefore the comparison between the two characteristic length scales of the medium: the total cross section in the n state, so the inverse of the mean free path in the n state, represents the length scale of the typical particle flight, while on the other hand the chord length represents the average linear size of the disorder of the material n. Having the condition in Equation 24 satisfied means, formally, neglecting disorder-induced spatial correlations, thus it is possible to replace the heterogeneous stochastic medium with a properly averaged, homogeneous one.

The opposite situation happens when the typical length scale of the disorder is much larger than the mean free path of the particle in that material. In this case, a great importance must be given to the position of the particle, since it will typically fly through a single material chunk.

Finally, the condition $\Lambda_n \cdot \Sigma_{t,n} \sim 1$, namely the condition in which the length scale of the randomness and the one of the particle flight are comparable, leads to not trivial behaviors. In this case the easiest way to describe the particle transport is using a probabilistic approach.

2.2 The Monte Carlo Method

The Boltzmann equation describes perfectly the physics of the phenomena involved in this work, but due to its complexity there is the need of a numerical method to solve it. In nuclear reactor applications we can divide these methods in two categories: deterministic and stochastics.

The deterministic method consists basically in the numerical resolution of the integrals and in the averaging of the physical properties of the system. Naturally, results are subject to approximations, but the number of operations is small compared to other methods, thus the computational cost is smaller.

With the stochastic Monte Carlo methods, instead, the aim is to find a way to simulate directly the phenomena, using statistical laws to describe the behavior of an ensemble of particles. This is in fact an excellent method to simulate the reality without approximations, but it has the drawback to require a lot of calculations to obtain a good accuracy.

The transport calculations in this work are done using Monte Carlo methods with the Monte Carlo transport code TRIPOLI-4®, developed in the SERMA department in CEA – Saclay.

Monte Carlo methods consist in the utilization of a repeated random sampling to obtain a numerical result. They are a huge ensemble of algorithms, and they are often used in physical and mathematical problems. The idea is to use statistical laws to describe a problem that could also be deterministic in principle, and this can be useful in cases where, due for example to the high number of free variables, it is difficult or impossible to have a deterministic solution.

As far as dosimetry calculations are concerned, the Monte Carlo method is a very useful tool, since there is no need to use geometrical approximations. In fact, it is possible to take into account the exact properties of the material interacting with the particles, and that leads to a precise evaluation of shielding effects and scattering processes.

2.2.1 Integral Estimation

The easiest form of the transport equation to be solved by Monte Carlo methods is the integral one. With Monte Carlo methods it is possible to solve definite integrals using an approach different from the deterministic ones. Taken R as our observable of interest, the evaluation of an inner product of the kind

$$R = \int_a^b dP \cdot g(P)\psi(P) \tag{25}$$

or, in higher dimension:

$$R = \int_V dP \cdot g(P)\psi(P) \tag{26}$$

can be done using the expected value:

$$E[f_P(P)] = \int_D dP \cdot f_P(P)P \tag{27}$$

Then, this expected value can be estimated as a sum given the law of large numbers. Indeed, according to the law of large numbers, for a random variable P distributed according to a law $f_P(P)$ and with finite expectation, the sum of the sample average will converge to the expected value as $N \to \infty$:

$$\frac{1}{N}\sum_{i=0}^{N} f_P(P_i) = E\left[f_P(P)\right] \quad \| \quad N \to \infty \tag{28}$$

Thus, taking a uniform probability density function in a closed interval $[a; b]$, the following expressions are valid:

$$\int_{-\infty}^{+\infty} f_p(P)\psi(P)\,dP = \int_a^b (b-a)\psi(P)\,dP = (b-a)E[\psi(P)] \sim \frac{1}{N}\sum_{i=0}^{N}\psi(P_i) \tag{29}$$

Even if this method can be not as efficient as other deterministic methods, such as Simpson or Gauss integration, Monte Carlo methods have proven to be a powerful tool to solve transport problems in stochastic media. Since the analysis requires the solution of a source problem, the equation solved by the code can be written as:

$$\begin{gathered}\Phi\left(\vec{r}, E, \vec{\Omega}\right) = \\ \Phi\left(\overrightarrow{r'}, E, \vec{\Omega}\right) exp\left[-\int_0^s ds'\Sigma(E)\right] + \\ \int_0^s ds' Q\left(\overrightarrow{r'}, E, \vec{\Omega}\right) exp\left[-\int_0^{s'} ds''\Sigma(E)\right]\end{gathered} \tag{30}$$

Since the presented study involves a parametrical analysis of the source, is possible to have an idea on how different kinds of geometry, disposition, density and shape can influence different parameters of the equation, such as the optical path length, and lead to different behaviors of the dose equivalent rate [14].

2.2.2 Central Limit Theorem

The Central Limit Theorem applied to Monte Carlo method is what makes possible to have a quantitative estimation of the accuracy of the results obtained with stochastic numerical methods.

In probability theory, the central limit theorem establishes that, in some situations, when independent random variables are added, their properly normalized sum tends toward a normal distribution even if the original variables themselves are not normally distributed. The variance (second order moment) of the random variables must be defined. The theorem is a key concept in probability theory because it implies that probabilistic and statistical methods that work for normal distributions can be applicable to many problems involving other types of distributions.

The convergence of the arithmetic mean of variables towards a Gaussian law does not imply that for a given number of terms, even very large, one can derive good confidence intervals (error bands). Other techniques, such as bootstrap, exist when the distribution of the mean converges slowly to the Gaussian law.

Taken $\frac{|\bar{\xi}^n-\mu|}{|\bar{\xi}^n|}$ as the relative error with respect to the exact result μ weighted on the sample average $\bar{\xi}^n$ and $\frac{\sigma}{\sqrt{N}|\bar{\xi}^n|}$ as the PRSD (Percentage Relative Standard Deviation), where σ^2 is the variance and N the number of random samplings, applying the Central Limit Theorem to the sample average $\bar{\xi}^n$ obtained by sampling a random variable ξ in a Monte Carlo experiment, we can obtain the expression:

$$P\left[\frac{\left|\bar{\xi}^n-\mu\right|}{\left|\bar{\xi}^n\right|} \leq \frac{k\sigma}{\sqrt{N}\left|\bar{\xi}^n\right|}\right] = \int_{-k}^{k} dt \frac{1}{\sqrt{2\pi}} e^{\frac{-t^2}{2}} \tag{31}$$

In practice, with this expression it is possible to have the exact probability value that the relative error on the result is smaller than the PRSD. The coefficient k is what gives the magnitude of the so called "Error Band", namely the interval of confidence of the results obtained with Monte Carlo methods. If $k = 1$, the interval of confidence of the simulation will be:

$$[\bar{\xi}^n - PRSD \cdot \bar{\xi}^n \ ; \ \bar{\xi}^n + PRSD \cdot \bar{\xi}^n]$$

And the integral of the second member of the equation (the so called "Error Function") is equal to around 0.68. That means that for a sufficiently large number of samples there is a probability of 68% that the exact result is contained in the interval of confidence. Extending the interval to $[\bar{\xi}^n - 1.96 \cdot PRSD \cdot \bar{\xi}^n \ ; \ \bar{\xi}^n + 1.96 \cdot PRSD \cdot \bar{\xi}^n]$, the probability that the exact result falls in the error band becomes 0.95 [15].

2.2.3 Transport Simulation with Monte Carlo

The first step to solve the transport equation with Monte Carlo is to define the Source event:

$$f(Q) = \frac{\mathrm{Q}(r_0, E_0, \Omega_0)}{\int\int\int \mathrm{Q}(r_0, E_0, \Omega_0) dr_0 dE_0 d\Omega_0} \tag{32}$$

where $\mathrm{Q}(r_0, E_0, \Omega_0)$ is the source function, and $f(Q)$ the normalized emission probability density function.

Once we know the initial position, energy and direction of the particle, we can study what happens to it. Here begins the second step: we have to track the particle.

The first thing to do is to compute the distance from the starting point to the first boundary of the geometry in the flight direction. The procedure is quite simple but depends on the way the geometry is described.

Taken ρ_{max} as the distance between the starting point and the boundary we can calculate the probability that the particle has to arrive at the boundary:

$$f(Q) = \frac{\mathrm{Q}(r_0, E_0, \Omega_0)}{\int\int\int \mathrm{Q}(r_0, E_0, \Omega_0) dr_0 dE_0 d\Omega_0} \tag{33}$$

where Σ_t is the total cross section of the medium. Obviously, this is the complementary probability to the one describing the events in which the particle does not reach the boundary:

$$P_{Collision}(\mathrm{r}, \mathrm{E}, \Omega) = 1 - \exp\left(-\int_0^{\rho_{max}} \Sigma_t(r' + \rho'_{max}\Omega, E) d\rho'\right) \tag{34}$$

To find the distance in which the collision happens, we can use the cumulative probability density function:

$$P_{Collision}(\rho|\mathrm{r}, \mathrm{E}, \Omega) = \frac{\Sigma_t(\mathrm{r} + \rho\Omega, \mathrm{E}) \exp\left(-\int_0^{\rho_{max}} \Sigma_t(r' + \rho'_{max}\Omega, E) d\rho'\right)}{1 - P_{Boundary}(\mathrm{r}, \mathrm{E}, \Omega)} \tag{35}$$

So we can sample the length of the flight of the particle, sampling

$$P_{Collision}(\rho|\mathrm{r},\mathrm{E},\Omega) = \Sigma_t(\mathrm{r}+\rho\Omega,\mathrm{E})exp\left(-\int_0^{\rho_{max}} \Sigma_t(r' + \rho'_{max}\Omega, E)d\rho'\right) \quad (36)$$

using the inverse transform method:

$$\rho = \frac{1}{\Sigma(r,E)}\ln(1-\xi) \quad (37)$$

where ξ is a random variable (this with values between 0 and 1). Once the travelled distance is randomly sampled, we can check if $\rho > \rho_{max}$. If it is, the particle has reached the boundary, and then boundary conditions are applied. If not, a collision at distance ρ has happened.

In case of collision, the algorithm is composed of three steps: first, we have to select the nucleus on which the particle collides. Then we have to sample the type of reaction, and, finally, in case of scattering or emission, we must assign new energy and direction values for the next path.

To select the nucleus where the collision happens, we firstly calculate the probability to collide with a single nucleus that belongs to a category k:

$$P_k = \frac{c_k\sigma_{t,k}(E)}{\sum_{k=1}^{N} c_k\sigma_{t,k}(E)} = \frac{\Sigma_{t,k}}{\Sigma_t} \quad (38)$$

So, intuitively, we must compute the ratio between the cross section of a single nucleus and the total cross section in the collision point. Then a random number ξ is generated, if its value is lower than P_k the particle will collide with the nucleus $k = 1$, otherwise we check if ξ has a value smaller than $2 \cdot P_k \quad (k = 2)$ and so on.

$$\sum_{i=1}^{k-1} P_i < P_k < \sum_{i=1}^{k} P_i \quad (39)$$

The second step is to choose the type of reaction. The approach is exactly the same: we construct a cumulative PDF around the ratio of the reaction cross section σ_k and the total cross section σ_t, then sample a random number ξ and look for a value of k that satisfies Eq. (38), where

$$P_k = \frac{\sigma_k(E)}{\sum_{k=1}^{N} \sigma_k(E)} = \frac{\sigma_k(E)}{\sigma_t(E)} \quad (40)$$

In the end, in case of a scattering reaction, pair production or any reaction that foresees a further history of the particle or the formation of new ones, we have to assign new values of energy and direction to all the particles involved.

In this specific case, the results will be obtained calculating the particle flux in a certain control volume, and then flux is multiplied by flux-to-ambient dose equivalent conversion coefficients to obtain the dose equivalent rate [16].

3 Monte Carlo Models Adopted

3.1 System Simulation

The entire system is simulated using the Monte Carlo transport code TRIPOLI-4®. The aim is to provide a parametric model that can be used to simulate different configurations of the same system. Thus, the typical geometry used for the simulation must contain all the shielding elements and all the radioactive sources that would be present in a typical glove box for nuclear fuel handling. In particular, the model foresees three radioactive source:

- A conic jar, containing MOX powder shielded by a stainless steel membrane and a mead envelope;
- A press table, with free powder upon it;
- A pellet container, made of molybdenum, with pellets on the inside.

The overall geometry is a parallelepiped of 500 cm by 200 cm and 450 cm high. The glove box measures 450 cm in height, but the base is reduced to 300 · 70 cm. A representation of the geometry obtained using T4g, namely the visual tool of the TRIPOLI-4® software, is shown in Figure 3 and Figure 4.

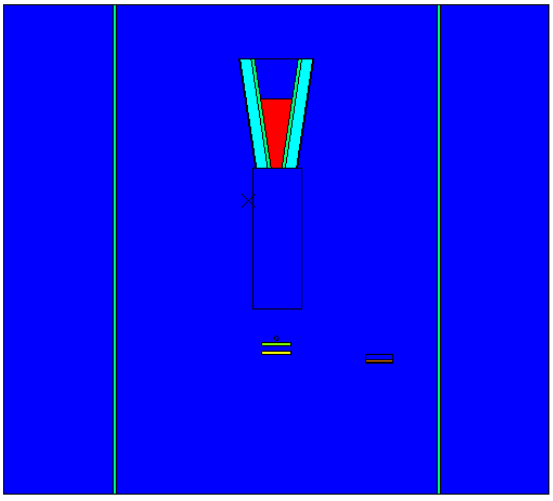

Figure 3: Glove box model on TRIPOLI-4®, view on the Y-Z plane. Each material corresponds to a color: RED: MOX, GREEN: stainless steel, BLUE: air, LIGHT BLUE: lead. The yellow rectangle, representing the tapis roulant, has the same composition of the MOX, but with a lower density. The blue circle just above the pressing table (green rectangle in the center) represents the detector for the internal dose equivalent rate.

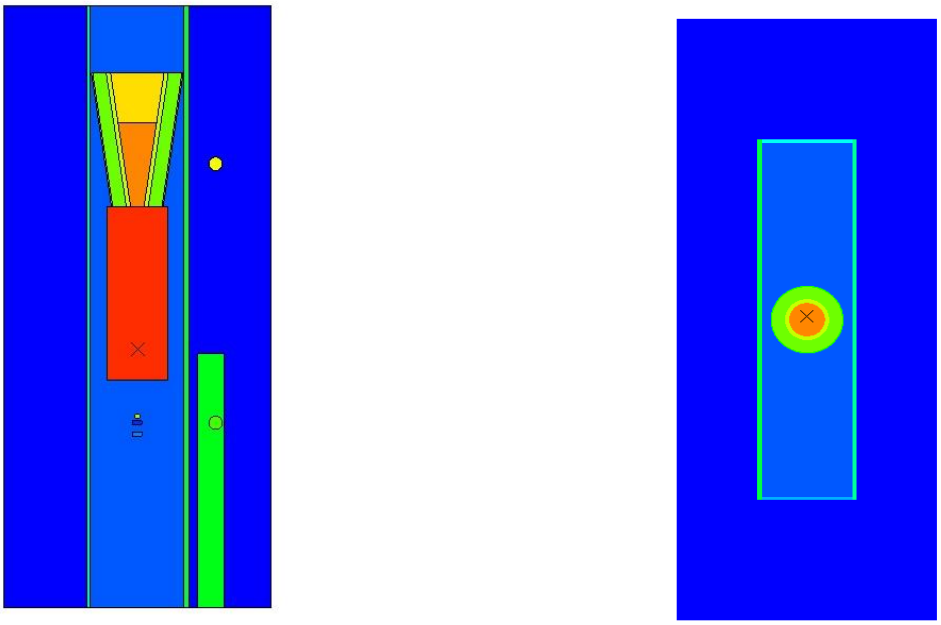

Figure 4: Glove box view on the X-Z plane (left) and on the X-Y plane (right). On the left figure the circles represent the detectors.

The shielding of these three sources for an external operator is provided by a stainless steel envelope and a Kyowa glass on the front face of the box. The Kyowa glass is a special acrylic-lead glass often used as shielding material for X-rays and gamma rays, a description and a list of physical properties, such the attenuation coefficient, can be found in [17].

The fuel considered for the simulations is a typical Mixed Oxide (MOX), whose composition is descripted in Table 2 [18]. As far as its composition is concerned, a percentage of radioactive isotopes comparable to the typical ones used in Light Water Reactors is used in the study to adapt the simulations to the highest number of possible scenarios.

Table 2: MOX Isotopes Mass Percentage. Data taken from the library https://www.nist.gov/pml/atomic-weights-and-isotopic-compositions-relative-atomic-masses on August 2019.

Isotope Name	**Percentage**
$^{235}_{92}U$	0.225
$^{238}_{92}U$	89.7
$^{238}_{94}Pu$	0.404
$^{239}_{94}Pu$	5.05
$^{240}_{94}Pu$	2.32
$^{241}_{94}Pu$	1.21
$^{242}_{94}Pu$	0.96
$^{241}_{95}Am$	0.152

With this composition it is possible to calculate both the mass density and the energy spectrum. The energy spectrum is calculated by the DARWIN-PEPIN 2® software [19], simulating one hundred grams of fuel. An observation should be done on the composition: most of the calculations are done assuming a constant percentage of the elements. In reality, we want to simulate also a hypothetical system that remains sealed for several years and where there's the possibility of radioactive dust accumulation, and this dust could exposed to high neutron fluxes. The temporal scale, in this case, should also be long enough in this situation to be able to appreciate the variation of composition due to the decay chain. The decay half life of each isotope is reported in Table 3. Since the aim of the work, more than a radiation protection analysis, is to highlight the differences between different models for the radioactive dust simulation, this aspect will be taken into account in a stand-alone experiment, but it will not play the a major role in the thesis.

Table 3: MOX Isotopes Half Life. Data taken from the library https://inis.iaea.org on August 2019.

Isotope Name	**Decay Half Life [y]**
$^{235}_{92}U$	4E+09
$^{238}_{92}U$	7E+08
$^{238}_{94}Pu$	87
$^{239}_{94}Pu$	2.4E+04
$^{240}_{94}Pu$	6.6E+04
$^{241}_{94}Pu$	14.3
$^{242}_{94}Pu$	3.7E+05
$^{241}_{95}Am$	4.3E+02

However, the model, as it currently stands, does not take into account the possibility of radioactive dust accumulation yet. Remembering that the aim of this model is not to describe an actual system but to provide an estimation of potential hazard, the radioactive dust is modeled as an ensemble of radioactive sources placed in the most critical spots of accumulation, and is simulated taking into account a wide range of parameters. As the radioactive source geometry describing the radioactive dust falls within the field of the disordered media, this modeling step is not straightforward. In the following sections the methods used to model the geometry are explained in detail.

3.2 Homogeneous Model

The simplest way to simulate a disordered medium is homogenizing it. The aim is to have a configuration with the same macroscopic properties as those of the real one, but a much more simple geometry. In the first analysis that uses the homogeneous model, the geometric shape of the source is fixed. Only the mass is variated parametrically, by changing the density of emitting volumes to simulate different dust densities. The radioactive material is supposed to be diluted inside a chosen volume larger than the volume actually occupied by the substance in the reality. Thus, instead of considering a disordered geometric arrangement of dense and compact dust grains, the radioactive dust will be simulated as a homogeneous source, with a simple

geometrical shape and a smaller density. This model provides the simplest way to insert into the system the exact quantity of emitting material at reasonable locations.

The process for a single simulation with the homogeneous model foresees three steps:

1. Source intensity calculation with the evolution code DARWIN-PEPIN 2®: the code receives in input the composition of the source material, and gives as output the emission spectra of neutrons and gamma photons.
2. Construction of the geometry: a Python script was written for this purpose. The code receives in input the desired location of the dust accumulation and the amount of mass to be simulated. The script returns as output a TRIPOLI-4® input file with the chosen source placed in the original glove box geometry.
3. Transport calculations: TRIPOLI-4® is used to carry out transport calculation. The output file of the simulation contains the values of the dose equivalent rate calculated in each detection spot.

3.2.1 Homogeneous Model – Parametrical Variation of the Source Density

The TRIPOLI-4® code receives as input, besides the geometrical setup, both the material composition and the emission spectrum. To create a homogeneous source, one must select a control volume containing the radioactive material. The density of this material is calculated as the mass of substance desired divided by the volume of the homogenized source:

$$\rho_{Homogeneous} = \frac{m_{source}}{V_{source}} \tag{41}$$

To calculate the source emissivity, the code takes as input the emission spectrum in particles emitted per seconds, divided by energy bands. The calculation is:

$$I = \#particles[g^{-1}s^{-1}] \cdot \frac{Angular\ Intensity}{4\pi} \cdot V_{source} \cdot COEFF\left[\frac{g}{cm^3}\right] \tag{42}$$

In this expression, $COEFF$ is a coefficient chosen according to the case: if a normalized emission spectrum is used, it must take into account both the mass density and the emission intensity. All the simulation are carried out with non-normalized spectra, calculated with 100 grams of fuel by DARWIN-PEPIN 2®. In this case, the term $\#particles[g^{-1}s^{-1}]$ should be divided by 100, in order to have the emission intensity for a single gram. The Angular Intensity is equal to 4π for the sake of simplicity, so the value of $COEFF$ is the mass density divided by 100, to correct the emission term. In case of neutron simulation, an additional arbitrary coefficient >1 could be added to consider the possibility of multiplication.

This operation and the effective creation of the geometry is done using the script Python described in the previous section, that calculates the density and coefficients for each value of the simulated mass and locates the sources at the right positions.

To choose the position of the dust sources, a few hypothesis are taken: first of all, assuming that the scenario in which an operator could operate in the glove box is a maintenance operation, it is assumed that all the machines have been shut down long enough for all the dust to settle on the surfaces of the box. This means that we suppose all the dust is attached to the walls, and its disposition does not change with time. In other words, flying dust is not considered. Neglecting buoyancy forces and considering gravity and electrostatic capture, the most probable accumulation spots are the Kyowa glass and the floor of the box. It is also assumed that, due to some difficulties in the routine cleaning operations, there is an accumulation in the bottom corners of the box [20]. In this analysis, the spots taken into account are the floor of the box, the Kyowa glass and the bottom corners, simulated, in this case, respectively with a thin parallelepiped - shaped layer which covers the floor or the Kyowa glass inside the glove box and two 5cm sided cubes to simulate the corners.

The limit of the model, perhaps, is the alteration of the properties of the medium on a microscopic scale. In fact, looking at the real case, we find dust specks with a really small average diameter [21], in the order of micrometers, dispersed in an air matrix [22].

3.2.2 Homogeneous Model – Parametrical Variation of the Source Thickness

The situation of atomic mix, in which it is reasonable to use a homogenization of the properties maintaining unaltered transport properties such as cross sections and sources, requires a mean free path longer than the length scale, or the chord length, of the geometry. From data found in literature [8, 23, 24] it is known that for some particles, such gamma photons, the mean free path in metals is very short. To get information about the length scale of the mean free path in our configuration, another experiment is carried on.

In this experiment the free parameters are the source thickness and the mass, while the density is fixed. To do this, the source is divided in several thin slices with a thickness that goes from $0.1cm$ to $0.005cm$, depending on the other parameters of the experiment. An example of the thin slices is shown in Figure 5. The analysis is carried out by adding these slices one-by-one: doing this, we will have a linear increase of the source term and of the source thickness. This method, derived from the homogeneous model, allows us to test if, in a system configuration, the superposition of the effect is valid. If this is true, trivially, the problem becomes linear, and the dose is simply proportional to the source intensity.

The procedure to carry out this kind of simulations is exactly the same as in the previous case, with the only exception that the Python script used to build the source geometry is slightly modified, in order to receive as input parameter also the thickness of the source volume.

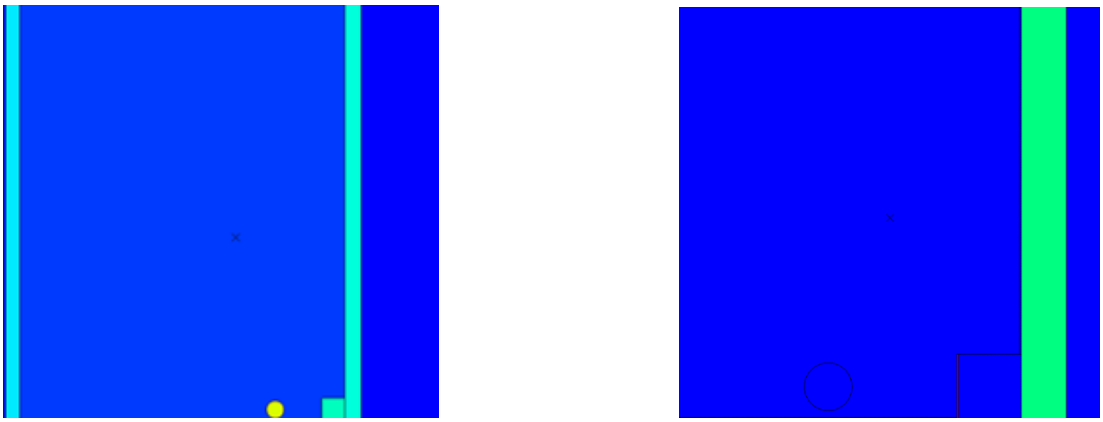

Figure 5: Position of the detector (left) and thin 1mm slice of MOX in the corner source (right).

3.2.3 Discrete Homogeneous Model for Flat Sources

The discrete homogeneous model was created to investigate if there are important differences between a flat source with an uniform mass distribution and sources with a variable density according to the position. A quick and easy method to analyze these possible differences is to create a bidimensional mesh, as shown in Figure 6, which divides the plane in small rectangles, and assign to each one of these rectangles a different mass value, according to a chosen probability density function.

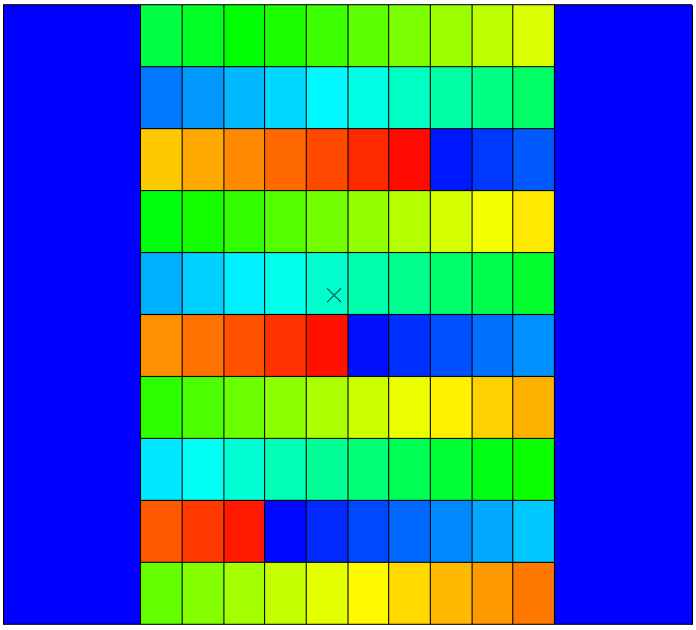

Figure 6: T4g plot of the Kyowa Glass Mesh.

This method is applied to the source representing the dust deposited on the Kyowa glass, since it is the widest one, and because the positions of the detectors with respect to this source can make this kind of study interesting. In fact, the Kyowa glass is the component of the glove box

which is the closest to the operator, and placing a higher concentration on its center may increase the dose equivalent rate measured on the original detector positions.

The first experiment with this model has the purpose of simply understanding the effect of the spatial distribution of dust on the dose rate measured, without choosing the disposition a priori. To do this, density values in each cell of the mesh are randomly sampled according to a uniform probability density function. We take as average density the value obtained with the pure homogeneous model:

$$\bar{\rho} = \frac{m_{tot}}{V_{tot}} \tag{43}$$

Then for each cell a density value is randomly sampled between the interval $[0.9 \cdot \bar{\rho}\,;\, 1.1 \cdot \bar{\rho}]$. The normalization condition is simply

$$\int_V dV\, \rho = \bar{\rho} V_{tot} \tag{44}$$

Which, since the domain is discrete, becomes:

$$\int_V dV\, \rho \sim \sum_{i=0}^{N} V_i \rho_i = \bar{\rho} V_{tot} \tag{45}$$

Since the mean value of the PDF is $\bar{\rho}$, there's no need to add further normalization coefficients.

A second experiment was done in order to obtain a greater concentration in the neighborhood of the center of the Kyowa glass with respect to the external part. A joint probability density function composed by two Gaussians was chosen for this purpose. The two monodimensional PDFs are in the form: $f(\lambda) = \frac{1}{\sqrt{2\pi\sigma^2}} \cdot exp\left[-\frac{(\lambda-\mu)^2}{2\sigma^2}\right]$ where the mean value μ correspons to the center of the Kyowa glass. Taken z as vertical coordinate and y as horizontal coordinate, the joint pdf can be written as:

$$f(y,z) = COEFF \cdot \frac{1}{\sqrt{2\pi{\sigma_y}^2}} \cdot exp\left[-\frac{\left(y-\mu_y\right)^2}{2{\sigma_y}^2}\right] \cdot \frac{1}{\sqrt{2\pi{\sigma_z}^2}} \cdot exp\left[-\frac{(z-\mu_z)^2}{2{\sigma_z}^2}\right] \tag{46}$$

Even if the Gaussian function is normalized by nature, since the domain is not infinite and the value are discretized, a coefficient $COEFF$ is added to normalize the function.

$$COEFF = \left\{ \frac{1}{N} \sum_{i=0}^{N} \frac{1}{\sqrt{2\pi {\sigma_y}^2}} \cdot exp\left[-\frac{\left(y_i - \mu_y\right)^2}{2{\sigma_y}^2} \right] \cdot \frac{1}{\sqrt{2\pi {\sigma_z}^2}} \cdot exp\left[-\frac{(z_i - \mu_z)^2}{2{\sigma_z}^2} \right] \right\}^{-1} \quad (47)$$

While keeping the mean values fixed, it is interesting to adjust the standard deviation to increase or decrease the peak of concentration in the center of the source and analyze the effects on the dose equivalent rate measured.

The condition the distribution must satisfy is again:

$$\int_V dV\, \rho \sim \sum_{i=0}^{N} V_i \rho_i = \bar{\rho} V_{tot} \quad (48)$$

In this case, the extended form of the sum becomes:

$$\sum_{i=0}^{N} V_i \rho_i = \sum_{i=0}^{N} \frac{1}{\sqrt{2\pi {\sigma_y}^2}} \cdot exp\left[-\frac{\left(y_i - \mu_y\right)^2}{2{\sigma_y}^2} \right] \cdot \frac{1}{\sqrt{2\pi {\sigma_z}^2}} \cdot exp\left[-\frac{(z_i - \mu_z)^2}{2{\sigma_z}^2} \right] \quad (49)$$

$$\cdot COEFF \cdot \bar{\rho} \cdot V_i = 1 \cdot \bar{\rho} \cdot \sum_{i=0}^{N} V_i = \bar{\rho} V_{tot}$$

The used methodology for this kind of calculations is very similar to the one used for the simple homogeneous model. The normalization coefficients are calculated by a Python script, which is the same used to create the mesh and the global system geometry. Then each simulation is carried on by using the TRIPOLI-4® code.

3.3 Random Sequential Addition Spherical Inclusion Method

In this case the approach is completely different: the simulation is not carried out by diluting the properties of the radioactive material inside a bigger volume, but by separating physically the radiation emitters (the dust grains) from the other materials, creating several independent spherical sources and dispersed in an air matrix. So this is a microscale approach, which falls into the domain of particle transport in disordered media. The basic Monte Carlo method to generate a stochastic inclusion of spheres is the random sequential addition method [25]: basically, what we want is to have a set of randomly distributed, non-overlapping spheres knowing the radius and the portion of volume we want the spheres to occupy. These spheres will be generated inside a chosen control volume, usually a cubic box, and this volume has to be defined according to what the case of study requires (for example using a control volume coincident with the one created for the homogeneous model simulation could be a good choice, if the aim is to compare the two models).

3.3.1 Monodispersed Radius Spherical Inclusions

In case of spherical inclusions with monodispersed radius, the number N of spheres to be generated is calculated as:

$$N = \left\lfloor \xi \cdot V \frac{3}{4\pi R^3} \right\rfloor \tag{50}$$

where ξ is the Packing Fraction of the inclusion, namely the ratio between the volume occupied by the spheres and the total control volume V(see 2.2.4), where the inclusions are generated.

Taken a cubic box as control volume, for spheres which cannot overlap the walls of the box, the random sampling of the first center of the inclusion is calculated generating, according to a uniform distribution, three random numbers within the range$\left[-\frac{L}{2}+R\,;\frac{L}{2}-R\right]$, where L is the size of the box and R the radius of the spheres.

The position of the first center is stored into an array, then another set of center coordinates is sampled. In this case the first step is to check if the last sphere overlaps with other existing ones. That is done using simple algebraic operations, in particular the distance between two points should be never smaller than the spheres diameter, and this has to be checked for each sphere. Naturally, the number of these operation increases sphere by sphere. This process is repeated until the number N of inclusions is reached.

The algorithm used in this work is an improvement of the random sampling additions method: it consists in the creation of a spatial mesh inside the control volume, with a dimension of the mesh cell greater than or equal to the diameter of the spheres. In this way, if we know the cell in which a center is situated, we have to check just the cells immediately close to find if there

are overlapping spheres. Furthermore, if a cell contains already a sphere, it can be excluded from the random sampling, since is impossible for two spheres in the same cell not to overlap [8]. An example of geometry obtained with this method is shown in Figure 7.

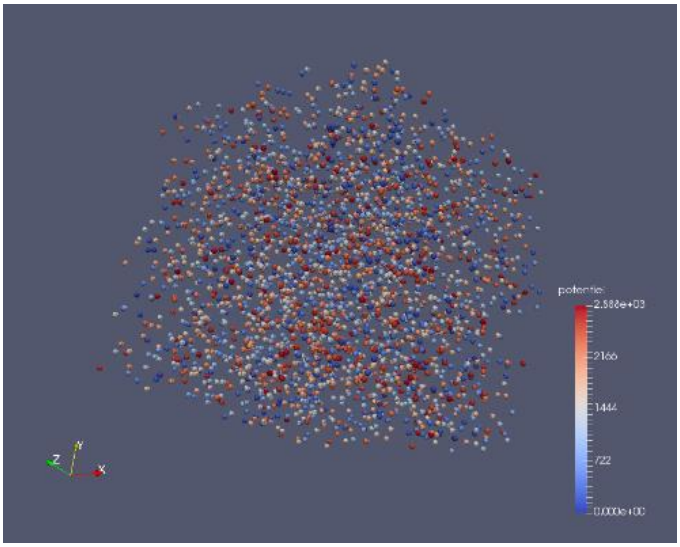

Figure 7: Paraview screenshot – monodispersed radius spherical inclusions in a cubic box.

With this kind of geometry there are three free parameters: the packing fraction ξ, the mass density and the radius of the spheres. It is thus possible to increase only the packing fraction ξ changing the source emissivity, directly dependent on the mass of radioactive material (so on the number of spheres), without changing the properties of each sphere. It is also possible to change the radius of the spheres and ξ, concurrently, the density of each sphere being constant modifying by this mean the transport properties without changing the source emissivity.

It is possible to dilate the very small spheres by decreasing the density of these spheres accordingly to obtain the correct emission factor for the sum of all spheres. However, this local homogenization approach may not give the exact same results as a simulation with the actual sphere diameters. This would change also the probability of special interaction with particles emitted by other sources. Moreover, this would change also the probability of special interaction with particles emitted by other sources.

To define the sources and the geometry for the transport simulation, in the case of monodispersed radius spherical inclusion the used process is not as trivial as in the homogeneous case. The emission spectrum is calculated with the evolution code DARWIN-PEPIN 2®, in the same way it is calculated in the previous cases. The stochastic disposition is generated separately with an appropriate code written in C++ language, that receives as input the packing fraction ξ, the size and shape of the volume containing the inclusions, the dimension of the cells of a mesh that can be created in the control volume (the cubic box correspondent to the old homogeneous volume for the corner source simulation) to accelerate the transport calculation and the radius of the spheres. The output of this code is a text file containing the information on the positions of the centers of the spheres and the mesh for the speed up. At this point, each sphere is positioned in the glove box with a Python script, and for each one a composition is assigned. For what concerns the source creation (more in detail in section 3.6), the Python script assigns to each sphere a control volume that, in this case, is simply a cubic

box circumscribed to the sphere, for the Monte Carlo sampling of the source. The control volume for the source definition could also correspond to the control volume for the generation of the spherical inclusions but, since in many cases the volume occupied by the spheres constitutes only a really small fraction of this last one, it is more efficient to assign a different control volume for the source sampling, and this, as said before, has to be done sphere by sphere. The general formula of the source composed by the N spheres is:

$$I_{Homogeneous} = \sum_{i=0}^{N} V_i \cdot \rho \cdot COEFF * \#particles[g^{-1}s^{-1}] \cdot \frac{Angular\ Intensity}{4\pi} \tag{51}$$

$$= V_{Homogeneous} \cdot \xi \cdot \rho \cdot \#particles[g^{-1}s^{-1}] \cdot \frac{Angular\ Intensity}{4\pi}$$

So the packing fraction has to be chosen according to the mass desired.

3.3.2 Poly-Dispersed Radius Spherical Inclusions

While spherical mono-dispersed radius inclusions are a good starting point for studying transport properties at the microscopic scale, spherical poly-dispersed radius inclusions allow for a better simulation of reality. Indeed, with this model it is possible to take into account the fact that dust grains do not have the same dimension. An example of geometry obtained with the poly-dispersed radius spherical inclusion method is shown in Figure 8.

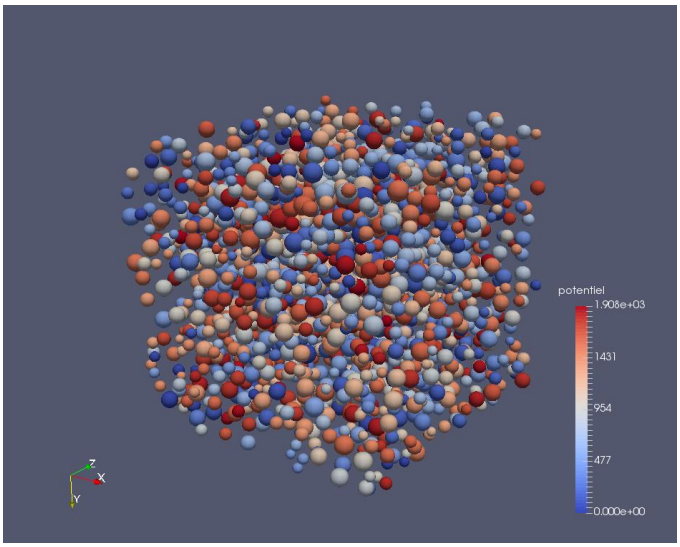

Figure 8: Paraview screenshot of a sample Poly-dispersed radius spherical inclusion, with a packing fraction of 10% and diameters uniformly distributed between 0.6 and 1.2 cm.

To obtain a binary mixture using this model, Random Sequential Additions method is used again [8]. The values of the radius are randomly sampled until a packing fraction greater than the chosen one is reached. At this point, the radius of the last sphere generated is modified in order to obtain the exact packing fraction ξ. Then the array containing them is sorted in decreasing order and the RSA method is applied. The idea is to find immediately a placement for the largest sphere in order to simplify the procedure.

For the simulation of the geometry with poly-dispersed spherical inclusions the procedure is similar to the monodispersed case, with the only difference that the values of the radius of the spheres must be randomly sampled from a distribution, or from a probability density function, before the inclusions are generated. Specifically, two PDFs are used for this purpose: a uniform distribution and a log-normal with mean value $\mu = 2{,}4\mu m$ and $\sigma = 0.84$. The last PDF is shown in Figure 9.

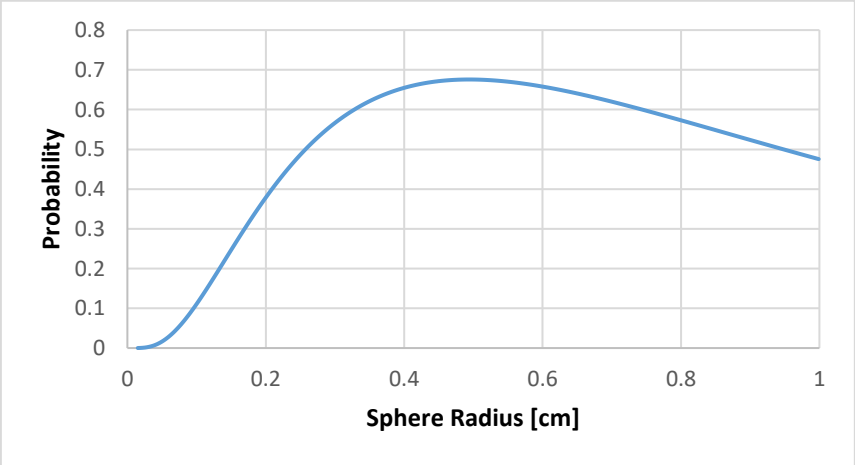

Figure 9: Log-Normal probability density function with mean value μ = 2,4μm and σ=0.84.

This value is taken from a former analysis on radioactive dust coming from pressing processes of MOX fuel [22]. The method chosen for the sampling according to a log-normal law is the rejection method. Naturally, also an inverse transform method could be possible:

$$f(r) = \frac{1}{r\sigma\sqrt{2\pi}} exp\left(-\frac{(\ln(r)-\mu)^2}{2\sigma^2}\right) \tag{52}$$

$$F(T) = \frac{1}{2} + \frac{1}{2} erf\left[\frac{\ln r + \mu}{\sqrt{2}\pi\sigma}\right]$$

$$r = \exp\left[\sqrt{2}\pi\sigma \cdot erf^{-1}(2\rho - 1)\right] - \mu$$

Where ρ is a random value between 0 and 1.

3.4 Other Stochastic Geometries

A different algorithm to generate spherical inclusions is proposed here. It consists in the construction of the most-dense packing of spheres possible, the so called Cannonball distribution, or cubic-face-centered lattice (CFC). A box is thus filled by a cubic-face-centered disposition of monodispersed radius spheres. Then, to shape the geometry, a rejection is applied, following different types of geometrical shapes. The last step, to obtain the mass desired, is a Russian Roulette, namely the stochastic elimination according to a certain probability, with the non-rejected spheres.

The lattice CFC is generated inside a cube $l \cdot l \cdot l$, to make this is possible to use the trigonometry formulas that link the position of the center of a sphere to the position of the center of the neighbors. This is quite trivial: on a single row the distance between two neighbor spheres is equal to the diameter of the spheres. In 2D, a lot of rows are superposed with a horizontal pitch with value $2r \cdot \cos(\frac{\pi}{3})$, while the vertical distance between a row and the other is equal to $2r \cdot \sin(\frac{\pi}{6})$. Finally, the same mechanism is followed for the third direction as for the second: each plane is spaced from the other planes of $2r \cdot \cos(\frac{\pi}{3})$ from the others, and each plane has a vertical and horizontal pitch with respect to the neighbor. To avoid overlapping of spheres through the walls of the cube, this procedure can be done excluding all the spheres whose center is at a distance smaller than their radius from the wall.

After the lattice is generated, to give it the desired shape, a mathematical expression of a geometrical figure is chosen to reject all the spheres contained, or not contained, inside it.

The simplest case is the rejection using a sphere of radius $r = l$ centered in one corner of the box. In this way it is possible to obtain a shape that is the entire cube minus an eighth of a sphere.

The analytical expression that the spheres have to satisfy not to be excluded is, thus:

$$0 < x_c < l$$

$$0 < y_c < l$$

$$0 < z_c < l$$

$$(l - x_c)^2 + (l - y_c)^2 + (l - z_c)^2 > l^2 \tag{53}$$

In this way, we obtain a volume of $l^3 - (\pi/6) \cdot l^3$ occupied by spheres with a packing fraction around 0.7. Since the aim of the model is to carry on parametrical analysis and creating source geometries comparable to those obtained with other models, we need to be able to choose the exact packing fraction of the inclusions. With an appropriate choice of the other parameters, having ξ equal to 0.7 can be good to simulate sources with high packing fractions, but this will lead to a number of volumes too large to be able to use TRIPOLI-4®. To manage the problem, and also add a stochastic component to the geometry, a Russian Roulette technique is applied to randomly reject unnecessary spheres, maintaining the shape of the geometry. To apply the Russian Roulette, a mass wanted m is chosen. In this case, with monodispersed radius of the spheres, this also leads to the wanted number of inclusions. The number of spheres needed to obtain that mass is thus calculated:

$$N = \left\lfloor m/(\rho \cdot \frac{4}{3}\pi r^3) \right\rfloor + 1 \tag{54}$$

If this number is inferior to the number of spheres already generated, we introduce the rejection probability $P_{Russian}$, which can be calculated either as $P_{Russian} = \frac{N}{N_{tot}}$ or $P_{Russian} = m/m_{tot}$, where N_{tot} and m_{tot} are respectively the number of inclusions and the total mass of the spheres before the rejection [26].After that, a random variable ξ is uniformly generated between 0 and 1 for each center of spheres, and all the spheres that do not satisfy $\xi > P_{Russian}$ are rejected and stored in a second array.

Once the loop for the rejection is finished, there is a final check on the number of remaining spheres: if that number is superior to the desired one, a new $P_{Russian}$ is calculated updating N_{tot} and m_{tot} and the rejection procedure is repeated. If, on the contrary, the number of inclusions obtained is inferior to N, the remaining centers to reach the number desired are randomly chosen from the array of the previously rejected spheres.

This algorithm, even if the stochastic nature of the geometry is partially lost due to the creation of the CFC lattice, gives us the possibility to shape the dust in a realistic way, and to have packing fraction way bigger than with the RSA method.

The shape of the geometry that is really close to the real shape is obtained by a first rejection method using three hyperbolic cylinders. In practice, the method is the same as before with the only exception that, to model the shape of the geometry, a different geometrical shape is used instead of the sphere octant. An example is shown in Figure 10.

The analytic expression of the volume is:

$$0 < x_c < l$$

$$0 < y_c < l$$

$$0 < z_c < l$$

$$0 < x_c < 4/z$$

$$0 < y_c < 1/x$$

$$0 < z_c < 1/4x$$

Figure 10: Representation of the geometry obtained from the intersection of the original cube with 3 hyperbolic cylinders.

3.5 Dust Aggregates Simulation

Dust grains often accumulate in the same place to form aggregates. It is interesting to see the difference between a modeling of a dust aggregate by homogenizing the properties on a single sphere and a modeling by a group of several objects of high density, glued together with an empty space between them. The process is exactly the same as the transition from the homogeneous model to the spherical inclusion model, but the length scale is considerably reduced. Dust grains are simulated with a hypothetic void fraction, and by averaging the properties it is possible to obtain an object with the global properties rather similar to a real dust aggregate. Moreover, since the mean free path of gamma rays inside the fuel itself is really small, we can deduce that the atomic mix limit, in our condition, is not satisfied in the single dust aggregate.

The following experiment has the purpose of giving an idea of the differences between the two modellings. It is carried out by creating an analytical distribution of spheres inside one bigger sphere, randomly placed in the geometry using the RSA method.

In this test the used geometry is a dense packing of twelve spheres, which has a packing fraction of about 42% with respect to the volume of the sphere in which the dense packing is contained (so the small spheres will occupy the 42% of the volume of the big sphere). It has to be noticed that the maximum packing fraction achievable with this kind of arrangement is around 49%, but due to some issue with the geometrical accuracy of the software it was necessary to add a small gap between each sphere. A representation of the dense packing of twelve spheres is shown in Figure 11.

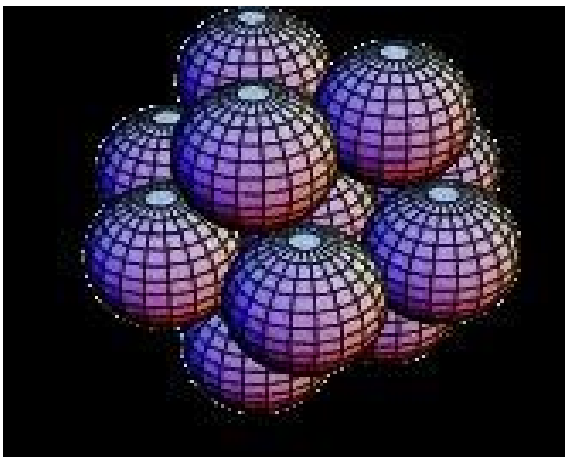

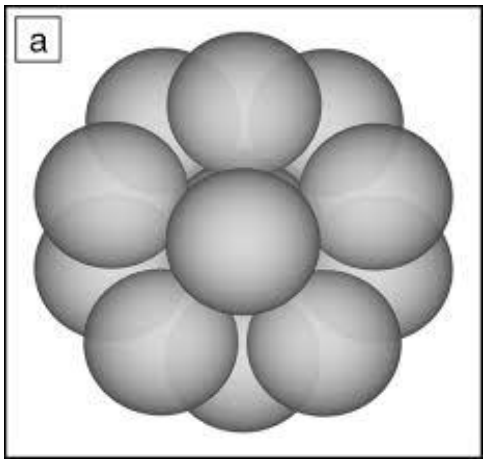

Figure 11: Drawings of the dense 12 sphere packing inside a bigger sphere.

In practice, the procedure to simulate dust aggregates is to generate a spherical inclusion inside a spherical inclusion. With the first generation it is possible to create a disposition of points randomly distributed with a minimum distance between each-others equal to the sphere diameter. The second inclusion, in this case, is not stochastic, but is obtained analytically using a Python script. Knowing the center of the packing, is possible to find relations that links the center of the aggregate to the center of the other spheres [27]: this geometry is indeed composed by spheres with the center that lay on the vertexes of two pentagonal-base pyramids with the bases touching each-others. The two pyramids also have a different orientation, with an offset of $\frac{\pi}{5}$.

The method adopted to simulate this kind of radioactive source is similar to the one adopted in the monodispersed spherical inclusions case. The Python script for the construction of the twelve spheres packing receives as input the output file of the C++ code for the spherical inclusions generation. In this way the geometry obtained is a stochastic distribution of aggregates composed of twelve spheres, and a second Python script is used to build the final TRIPOLI-4® input file with this source placed in the bottom corners of the glove box.

Using the code TRIPOLI-4®, in this way, is possible to simulate two objects of different kind: a dense aggregate of twelve spheres or a big sphere with a void fraction physically existent in the object, so simply the first geometry with the material properties exchanged.

3.6 Sources Handling in Stochastic Geometries

The major issue with a dispersed source, in Monte Carlo simulation, is the convergence of the source itself. Since the simulation of the particle transport is carried out by a Markovian random walk, the source coordinates are fundamental, since the starting point of the random walk is randomly sampled inside the source volume.More precisely, the declaration of a source consists in giving the code the coordinates of a mesh parallelepiped, and information to indicate whether or not the volumes within this parallelepiped are emitting. In this way, the code randomly

samples a given number of points inside the parallelepiped, and if that point falls into a fissile volume another random sampling begins to choose energy and direction of the particle. So, the process with which the starting point of the random walk is chosen is a rejection process [16]. It is trivial to understand that for this reason we would not have issues with homogenized sources, since the rejection efficiency is equal to the ratio between the volume of the parallelepiped used as a control volume and the volume of the source itself:

$$\eta_{rejection} = \frac{V_{source}}{V_{control}} \tag{55}$$

In the case of the homogeneous model analyzed in this report, it is possible to have always $\eta_{rejection} = 1$, since all the sources are, for simplicity, parallelepiped-shaped. Things change using more complex geometry sources: to analyze the transport inside a very dispersed source, so without the dilution of the properties in the whole control volume, but separating physically the fissile volumes from the air matrix, we could have to handle situation in which the fraction of the volume occupied by the source is less than the 1% of the total volume. Since is fundamental to have a good convergence of the source, looking at the Central Limit Theorem derivation for Monte Carlo [15]:

$$P\left[\frac{|\bar{\xi}^n - \mu|}{|\bar{\xi}^n|} \leq \frac{k\sigma}{\sqrt{N}|\bar{\xi}^n|}\right] = \int_{-k}^{k} dt \frac{1}{\sqrt{2\pi}} e^{\frac{-t^2}{2}} \tag{31}$$

it is immediately clear that we would need an enormous number of random samplings to obtain a good accuracy. Furthermore, the probability of success of the sampling is very close to zero, so there can be huge fluctuations in the sample average value. The solution is to improve the efficiency of the rejection by taking, for each sphere, a cubic cell in which a single sphere fits perfectly instead of a single large control volume.

In this case we have a great improvement of the efficiency, which, using Eq. (55), becomes:

$$\eta_{rejection} = \frac{V_{source}}{V_{control}} = \frac{4\pi r^3}{3 \cdot 8r^3} = \frac{\pi}{6} \tag{56}$$

The maximum packing fraction achievable with the RSA method is $\xi_{MAX,RSA} = 0.38$, and using the same control volume for the generation of the spherical inclusion and for the sampling of the source means having an efficiency coincident with the packing fraction (see Eq. (54)). Since the efficiency calculated in Eq. (56) is higher than $\xi_{MAX,RSA}$, using a single cubic cell for each sphere will always lead to an improvement.

It is also possible, however, to have efficiencies smaller than $\eta_{rejection} = \frac{\pi}{6}$ without any problem and, as a rule of thumb, the limit of the minimum rejection efficiency can be fixed around $\eta_{min} = 0.1$.

And since having less control volumes means speeding up the simulation, an approach using a control volume for each emitting volume of the source is avoided as often as possible. For example, in the case of the spherical inclusions built using a CFC lattice it is convenient to choose directly the entire control volume as rejection volume, since usually the packing fractions are very high. In the case of the use of the same method, but shaped with particular geometrical figures (for example the spherical or the hyperbolic shapes), it is possible to use some parallelepipeds to build a rejection volume around the source to fit this last one in the closest way possible.

Concerning the simulation of aggregates, luckily, the packing fraction inside the spheres is quite high (around 42.4%), so by using the same method as that used for the stochastic spherical inclusions, it is possible, according to Eq. (55), to have a rejection efficiency equal to

$$\eta_{rejection} = \frac{V_{source}}{V_{control}} \xi'$$

where ξ' is the packing fraction of the second spherical inclusion. So, in the case of a dense packing of twelve spheres inside a sphere, we got

$$\eta_{rejection} = \frac{V_{source}}{V_{control}} \xi' = \frac{4\pi r^3}{3 \cdot 8r^3} \xi' \sim \frac{\pi}{12} \tag{57}$$

These optimization procedures gain a great importance when the number of spheres becomes very large. In particular, to avoid computational times of the order of months, there are three separate phases of the simulation to be optimized.

The first one is the reading of the geometry: simply, the code controls that the geometry is convex, and creates maps that will be useful for the next phases. The second one is the source initialization, in which for each control volume declared the random sampling of points happens to calculate the effective magnitude of the emitting volume and also to find the intensity of the source contained in that volume. Last but not less important, the transport, in which a fixed number of random walks start from the sources: that is the process in which the code is able to store some parameters, like collision densities, and to provide the numerical results of interest. From here a series of complications derives by the fact that the simulation carried out contains even millions of volumes: firstly, the code has to verify that millions of volumes are effectively contained into a convex geometry. This operation is obviously done point by point, and during this operation the volumes are mapped, starting from the first one declared until the last one. Then, the code constructs a connectivity map: this is a list that associates to each volume of the geometry its closest neighboring volumes. Is very useful to speed up the transport operations, since knowing the neighborhood of a point allows the code to reduce drastically the control operations. At this point, after the research on nuclear libraries of the material properties, the source initialization begins. A great issue in this phase is the fact that each source volume is

searched inside the volume map, and this can give problems when the volume map contains millions of elements. In the end, the transport begins, and having a lot of volumes means a lot of operations to sample the starting points of random walks (fissions and gamma emissions happen in the fissile materials, with a dispersed source finding a point in which the material composition allows a particle emission can require a lot of samplings) and continuous changes of the material properties for the particle-material interactions (having a binary mixture means changing, also several times, the material crossed by the particles during their flight).

The solutions for these problem are not trivial: to avoid the problem of the geometry reading, it is sufficient to test the convexity of the geometry using a sample case with less volumes, with a disposition obtained with the same algorithm to be used in the real simulation. Once we are sure that the geometry is convex, is possible to remove the testing of the geometry in the code.

In the source initialization phase, to allow the code to bypass the control of the source volumes by searching them in a tree map, a modification of the code was necessary, and a specific function that allows to do this operation without checks on that map was implemented in the TRIPOLI-4® code.

In the end, in the transport phase, it is possible to accelerate the process creating a connectivity map specific to the situation. To do that is useful creating a mesh inside the volume containing the stochastic inclusions, in order to separate a larger volume containing a huge number of elements in several volumes containing just a fraction of them. The connectivity map itself is just the list of the volumes present in the geometry coupled with their neighbors. In this way, each sphere has almost 8 neighboring elements, since it cannot overlap to other spheres and can be present in a maximum of 8 mesh cells simultaneously, while each mesh cell contains a lot of spheres. The mesh is useful also for the definition of the interface between the system glove box and the source volume: since we imposed that a sphere cannot overlap the walls of the volume in which itis generated, the only contact between the glove box and the source is represented by the external cells of the mesh.

3.7 Time Dependent Scenario

The study is carried out supposing that the mean accumulation rate of the radioactive dust inside the glove box is estimated around 30 grams per year. It can be interesting to analyze the differences between a model that does not take into account the ageing of the radioactive dust and a model that does. The aim of the experiment is to study the effect on dose of the ageing of radioactive dust over a period of time. It is assumed that the dust has accumulated for some time (10 years for example).

The fuel properties in function of the age are discretized taking into account a time step of one year, for a total duration of 10 years. Since the accumulation rate is considered progressive, with a constant rate, is logic to think that every year 30 grams of fresh fuel powder are deposed in the corners of the box, while the pre-existing dust is subjected to some processes of nuclear transition, such the radioactive decay.

The emission spectra of the fuel after a fixed time are calculated again using the code DARWIN-PEPIN 2®. Once the spectrum of the fuel after a certain decay time is calculated,

two different approaches are used to calculate the total emission source, according to the used model.

With a model that uses separate volumes (spheres) to simulate the source the process is quite trivial: taken N as the mean number of volumes deposited in one year, during the first year we have an accumulation of N volumes, with an emission spectrum that is the average of the spectrum of the fresh fuel with the one-year-old fuel. The second year, there is the addition of other N volumes with the same properties, but the first N spheres will have 1 year more. So, to simulate this, it is sufficient adding N spheres with an emission spectrum calculated one year later to the preexisting N. The procedure is repeated until 10 years.

With a homogenized volume model, it is possible to use the fact that in the Monte Carlo code the emission spectrum is discrete to have an average value of number of emitted particles per each energy band. The input quantity, in the TRIPOLI-4® code, is the quantity of particle emitted per gram of material per energy band. Using an average spectrum, and giving the code the mass density and the volume of the source, we obtain the total number of particle emitted by the source every second, and the approximated emission probability for each energy level. In the results section it will be showed only the results of the homogeneous model, because they are sufficient to understand the differences between the steady-state and time dependent situation.

4 Results and Discussion

All the results are provided in terms of radioactive dose equivalent rate DED H(10) [28], expressed, using unity of measurement of the International System, in $\mu Sv/h$. Each source volume is simulated separately from the others, with the exception of the source representing the dust in the corners, which has two emitting volumes. This means only that we do not consider the emission of particles from the two separate sources at once: other transport effects, like absorption, are taken into account by giving to each component of the system its exact material composition, and so the real cross section values. In this way it is reasonable to assume that we can obtain the total dose rate coming from more than one source simply summing up the different contributions.

Due to the stochastic nature of the calculation process, the values of relative standard deviation of the results will be provided in each section. The main convergence problems concern the gamma dose calculations outside the glove compartment, as the shielding of the Kyowa glass and the other radiological protections does not provide a sufficiently large gamma particle sample. The convergence of neutron calculations does not pose any particular problem.

The analysis is in particular focused on the dust contribution inside the glove box (extremity dose for the hands of a hypothetical operator working, or dose calculated in chosen points really close to the source), since there is no shielding from gamma rays and the dose rate due to this additional source can be important.

4.1 Preliminary Calculations

To calculate the dose equivalent rate at which an operator is exposed without taking into account the possible radioactive dust, the three big radioactivity sources presented in the glove box must be considered. Six simulations are carried out: two for each radioactive source, one for the emission of gamma photons, another one for the emission of neutrons and photons coming from n, γ reactions. For the neutron calculations, in the analysis of the jar, a multiplication coefficient is taken into account for safety reasons: previous studies carried on by CEA on this system fixed this coefficient equal to 1.24.

Three detection spots are used in this study: one just above the press, inside the glove box, and two outside the box, placed in front of the Jar and in front of the Press. Not all the calculations are trivial: while neutrons have a good probability to pass the barriers and reach the detectors, providing a sufficiently large amount of samples to obtain a good standard deviation, gamma photons are very well shielded by both Kyowa glass and metal casings. The results of the simulations are reported in Table 4, and the PRSD of the results in Table 5.

Table 4: Preliminary Analysis – Dose equivalent rate measured in each detector considering each source.

Dose Equivalent Rate H(10) [$\mu Sv/h$]	**(n, γ) Photons**			**Neutrons**			**Gamma Photons**		
	Jarre	**Nacelle**	**Presse**	**Jarre**	**Nacelle**	**Presse**	**Jarre**	**Nacelle**	**Presse**
Source Intensity [particles/s]	2.68E+06	2.16E+05	1.11E+04	2.78E+06	2.24E+04	1.11E+04	2.66E13	2.13E12	6.40E+10
Detector in front of the Press	3.12E-02	9.33E-03	8.04E-05	1.10E+00	2.03E+00	3.32E+00	6.76E-02	3.24E-01	1.50E-01
Detector in the Gloves zone	9.74E-02	2.91E-02	3.54E-03	8.97E+00	8.02E+00	2.38E+02	1.16E+01	4.51E+00	1.10E+03
Detector in front of the Jar	5.62E-01	3.40E-03	1.54E-05	1.99E+01	2.53E-01	1.49E-01	9.07E-01	7.66E-02	5.36E-03

Table 5: Preliminary Analysis – Dose equivalent rate measured in each detector considering each source – Standard deviations.

PRSD	**(n, γ) Photons**			**Gamma Photons**			**Neutrons**		
	Jar	**Basket**	**Press**	**Jar**	**Basket**	**Press**	**Jar**	**Basket**	**Press**
Detector in front of the Press	4.47E-01	3.57E-01	1.36E-01	9.49E+00	3.85E+00	1.35E+00	3.68E+00	2.54E-01	1.46E-01
Detector in the Gloves zone	1.72E+00	1.30E+00	1.34E-01	7.06E-01	6.45E-01	1.00E-01	2.97E+00	1.47E-01	1.40E-01
Detector in front of the Jar	1.60E-01	6.15E-01	6.15E-01	9.18E+00	5.50E+00	5.55E+00	1.02E+00	5.67E-01	4.03E-01

The largest dose equivalent rate is registered above the press, since it is the spot closest to any radioactive source, and since the powder composing the source is completely unshielded. In that case, the major contributors are the gamma photons, since a great number can easily reach this detection spot. Things change looking at the external detectors, where neutrons are more important, since they have a bigger mean free path in the shielding materials (see Figure 4). Table 6 shows the global dose equivalent rate calculated in each detection spot.

Table 6: Preliminary Analysis – Global dose equivalent rate calculated in each detector.

Dose Rate H(10) $[\mu Sv/h]$	All Particles			Total H(10)
	Jar	Nacelle	Press	
In front of the Press	1.20E+00	2.36E+00	3.47E+00	**7.03E+00**
In the Gloves zone	2.07E+01	1.26E+01	1.34E+03	**1.37E+03**
In front of the Jar	2.13E+01	3.33E-01	1.54E-01	**2.18E+01**

It is possible to calculate the percentage of the contributions of gamma and neutrons inside and outside the glove box casing. These percentages are reported in the cake plots in Figure 12.

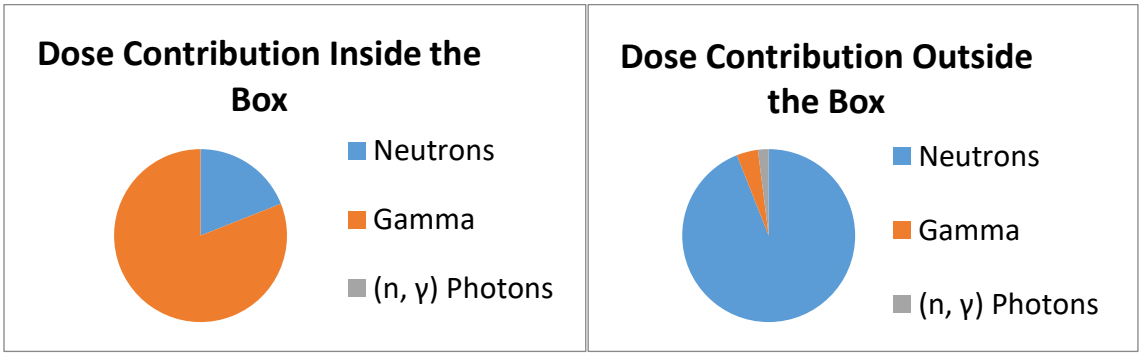

Figure 12: Cake plots showing how each particle influences the total internal and external dose equivalent rate in the glove box.

4.2 Homogeneous Model

The first analysis using the homogeneous model is performed taking into account a wide range of mass values, since the objective is to have an estimation of the potential hazard provided by each deposition spot. The mass present in each source is varied parametrically starting from a very small mass to a value comparable to the mass of dust on the pressing table (situation that can represent, for instance, an accidental scenario or the EOL of the machine, when there is the presence of dust accumulated for years). The density values obtained in this way can vary from the order of magnitude of the PM concentration in a polluted big city, such as Paris, to a value similar to the yellowcake density. Naturally the transport properties change a lot, as the diffusion of particles is influenced by the macroscopic cross sections of the medium, that directly depend by the number of nuclei on the path of the particles (quantity that is directly correlated to the mass density). This effect will be better investigated in the section 4.2.2.

4.2.1 Parametrical Variation of the Source Density

These first results, representing the behavior of the dose rate measured inside the glove box, so without the shielding provided by the envelopes, show that variating the density of the source a saturation effect happens on the dose due to gamma rays. This, perhaps, happens only when considering the corners and the bottom edge. The reason of this saturation is the increase of the absorption cross section of the source itself, which makes impossible for the particle with a short mean free path to come out from the medium [29]. While neutrons have a very long mean free path compared to the source dimension [30], gamma rays are very well shielded by the metals. The results are shown in Figure 13, Figure 14, Figure 15 and Figure 16.

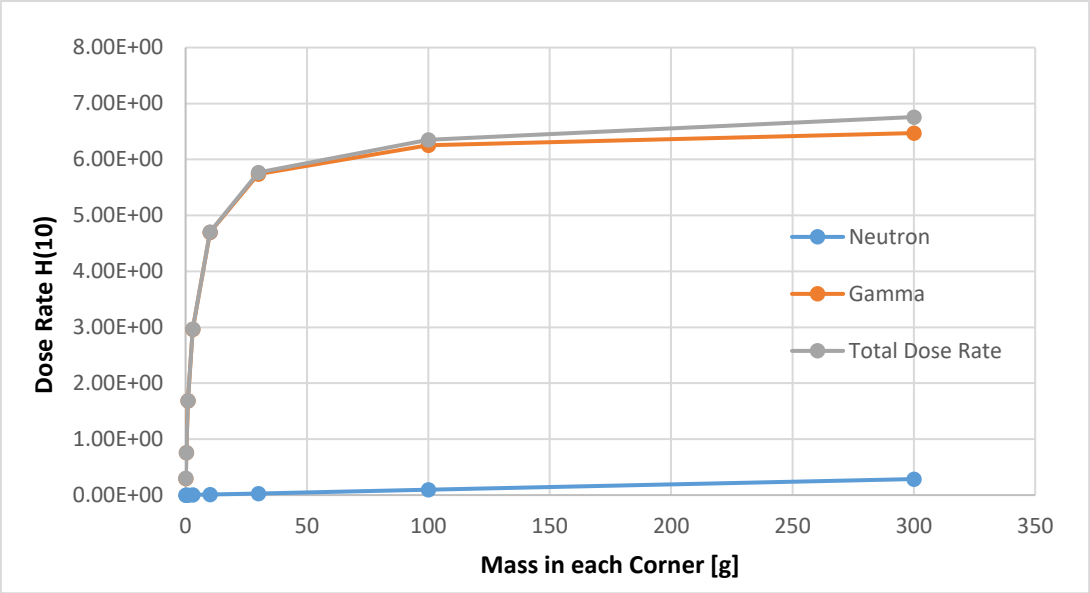

Figure 13: Homogeneous model, corner source with parametrical variation of the density, calculations above the press.

Simulations for the corners of the glove box are done using two $5 \cdot 5 \cdot 5\,cm$ cubes as homogeneous volume for the "dilution" of the dust material. Thus the parametrical analysis with a mass range between 0.1 and 300 grams will have a density range that goes from $0.0008\ g/cm^3$ to $2.4\ g/cm^3$. In general, simulations for neutron dose are done using 20000 batches of 3000 particles each one and at least 300000 batches of 5000 particles for gamma dose. While with neutron calculations the standard deviation obtained is similar case by case, for gamma calculations the convergence speed decreases with the increase of the density, due to the reduced quantity of particles that are able to escape from the source.

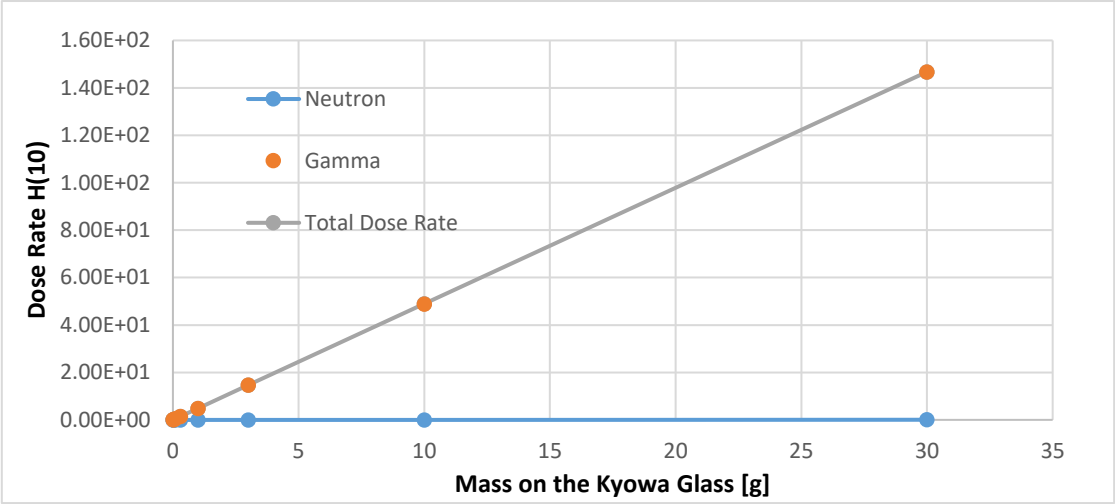

Figure 14: Homogeneous model, Kyowa source with parametrical variation of the density, measures above the press.

The dust on the Kyowa glass is simulated using a thin film,$0.1 \cdot 300 \cdot 450 cm$, that perfectly covers the internal surface of the glass. Here the behavior of the dose rate is completely different, since the source analyzed is, in practice, a flat source. Simulations are done using 20000 batches of 3000 particles for the neutron dose calculations and 300000 batches of 5000 particles for gamma rays. Here the convergence speed is not influenced by the density of the medium, but only by the detector position. The amount of simulated mass goes from 0.01 g to 30 g, a smaller quantity with respect to the corners, since a smaller amount of dust is expected to be deposited on the Kyowa glass.

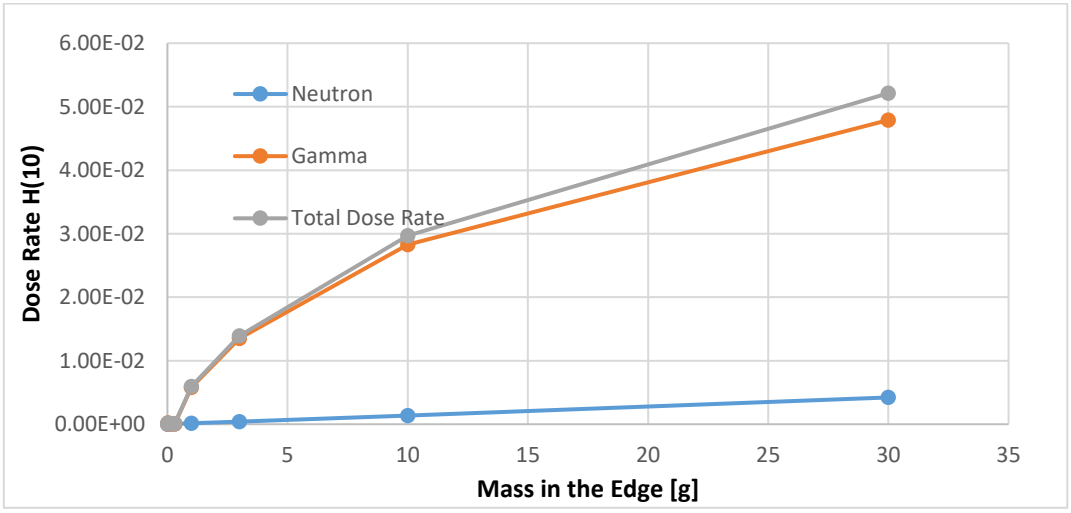

Figure 15: Homogeneous model, bottom edge source with parametrical variation of the density, calculations above the press.

The edge of the glove box is simulated using a $5 \cdot 290 \cdot 5\ cm$ parallelepiped. Even if the control volume chosen is not totally realistic, it was chosen anyway to compare the dose curve obtained with a parallelepiped-shaped source of larger volume than the one obtained with the corner source. The mass range is the same used for the corner source, but diluted in a volume 58 times larger. In fact, the saturation effect is always visible, but the slope of the curve is higher with respect to a more compact deposition. The parameters of simulation used with

TRIPOLI-4® are the same as for the corner source. In this specific case, the convergence of gamma dose rate at high mass values is faster, because of the decrease of absorptions (due to the lower mass density).

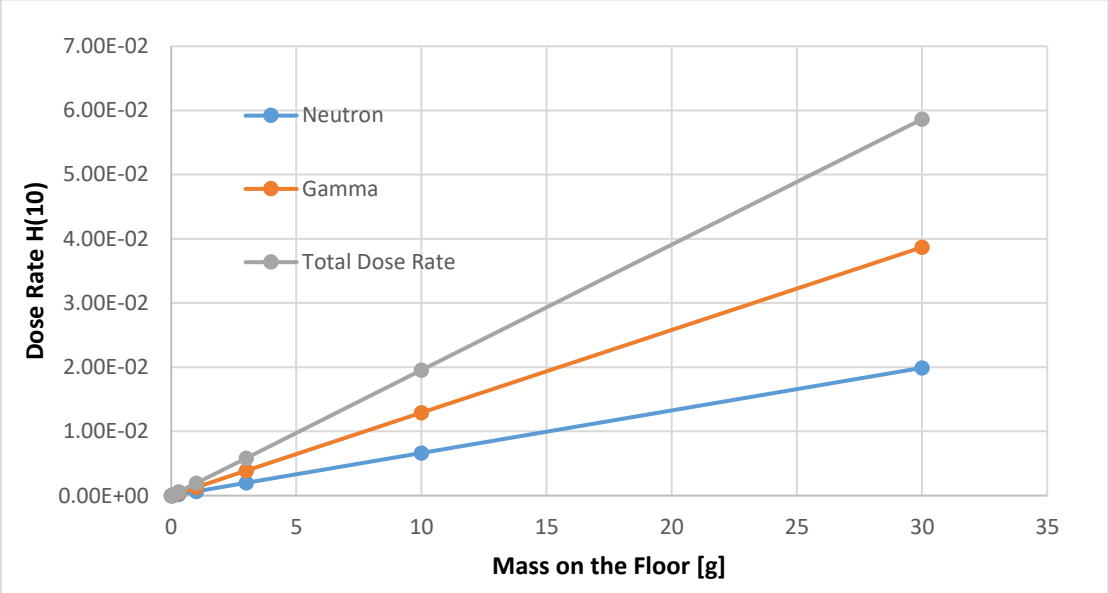

Figure 16: Homogeneous model, floor source with parametrical variation of the density, calculations above the press.

The floor source is simulated as a $70 \cdot 300 \cdot 0.1\ cm$ thin layer placed at the bottom of the glove box. All the considerations made for the source due to dust on the Kyowa glass are valid, except for the greater distance between the source and the calculation point, which reduces the dose. Even if this source is placed on the floor, the range of mass values considered is the same as for the Kyowa glass. Indeed a smaller amount of dust is expected far from the corners and the edge of the box, due to the frequency and effectiveness of cleaning operations in this area.

It has to be noticed that for radioactive sources at ground level, this calculation is influenced a lot by the shielding effect provided by the press and the pressing table. To better understand the influence of the shielding effect provided by the press and to find the minimum distance to be respected between the press and the detector to avoid this problem, a further experiment was carried out. Taking into account the source composed by the corners of the box, the dose equivalent rate is tracked in 11 points distributed along the vertical axe of the glove box. Two configurations are simulated the first one with the original materials in the box and the second one with the glove box without the press. The two configurations are visible in Figure 17.

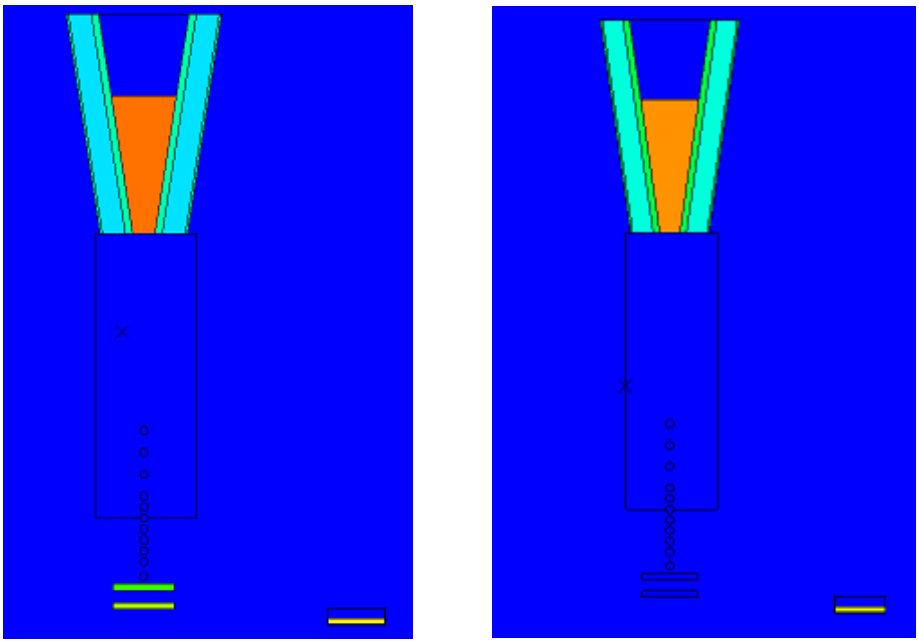

Figure 17: Image representing the two configurations, each color corresponds to a specific material. On the left, the 11 detection volumes are visible above the press and the treadmill with their original composition. On the right, without the press.

The results of the simulations, normalized to the first dose equivalent rate value where the results of the two experiments converges, are reported in Figure 18:

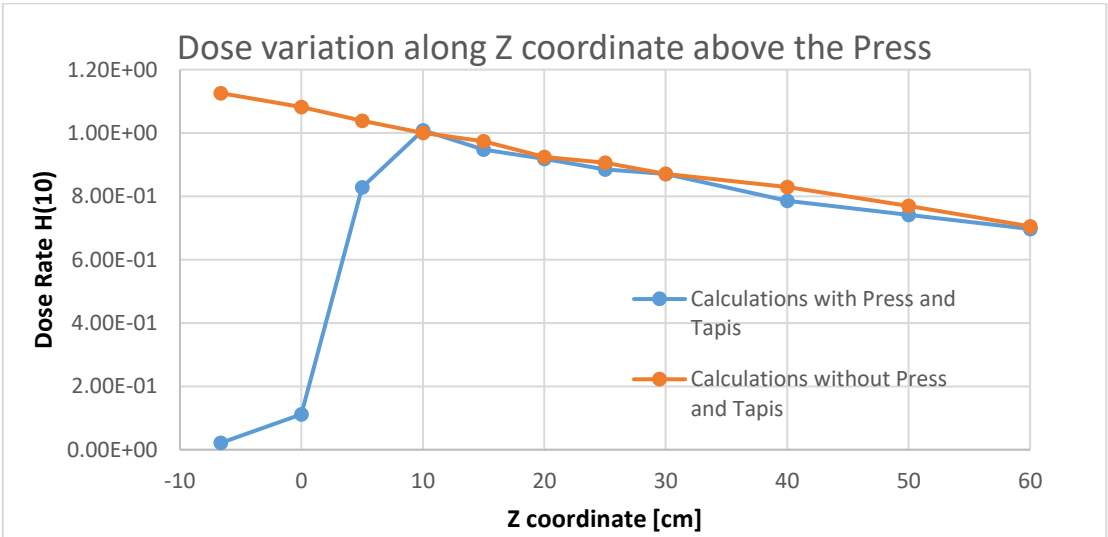

Figure 18: Influence of the press shielding in function of the quote of the detector.

Therefore, the dose calculated keeping the detector in the same position as in the previous calculations (without radioactive dust) there is a decrease of the calculated dose of about the 20%.

The contribution to the dose equivalent rate in the external part of the glove box, using the same detection spots used in the simulations of the original system, is less important, thanks to the shielding provided by the glass of the glove box. For what concerns the analysis of the corner source, the dose equivalent rate calculated outside the glove box at the press quote is shown in Figure 19, while Figure 20 contains the results obtained calculating the dose outside the glove box at the jar quote.

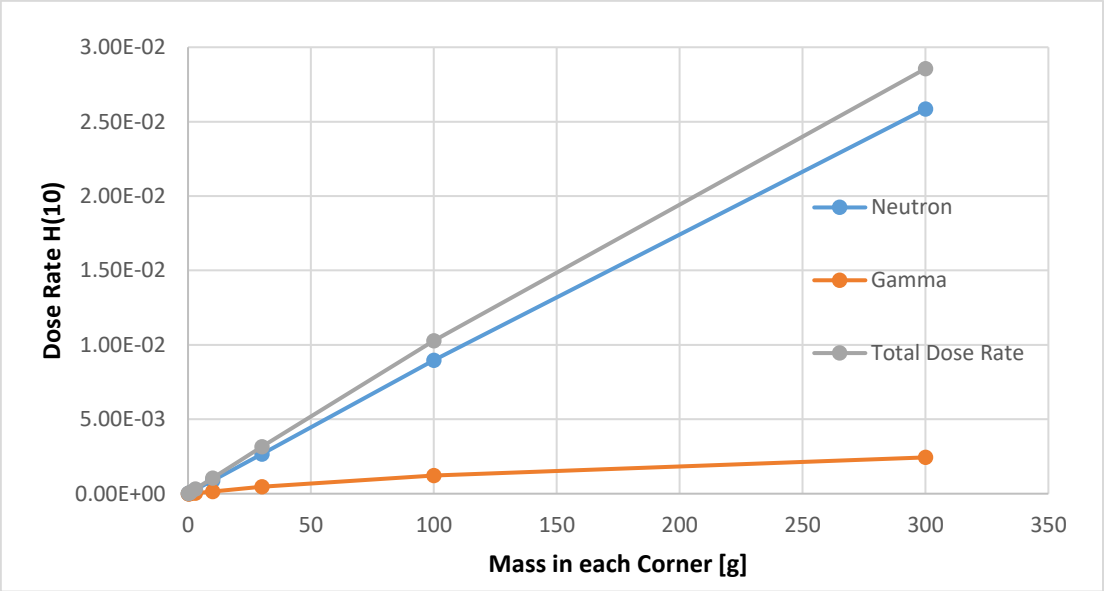

Figure 19: Homogeneous model, corner source with parametrical variation of the density, calculations outside the glove box at the press quote.

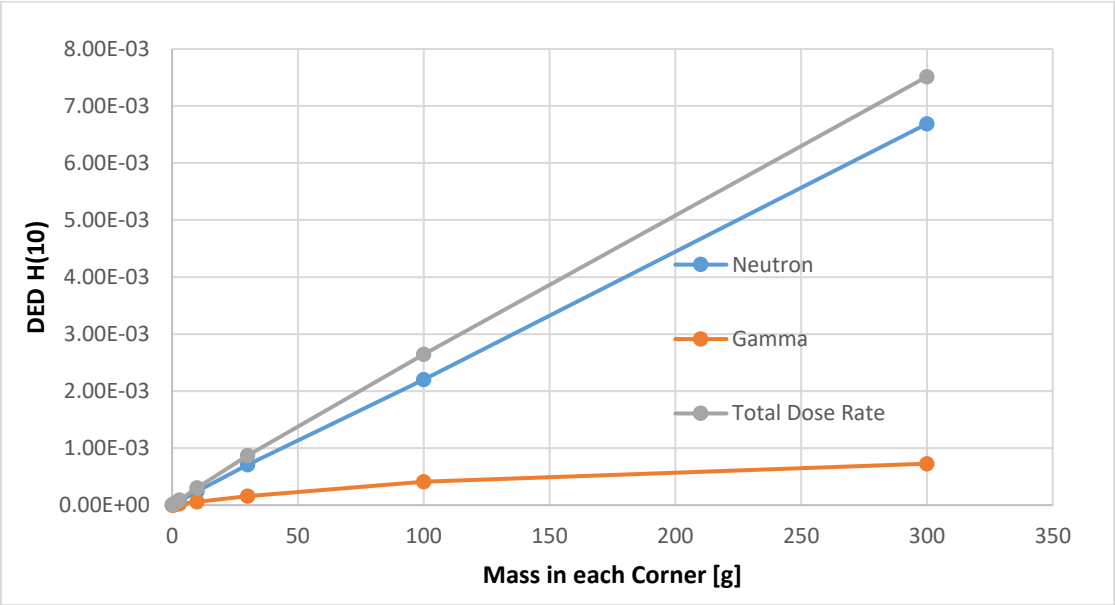

Figure 20: Homogeneous model, corner source with parametrical variation of the density, calculations outside the glove box at the jar quote.

Since the source volumes for the corners are placed on the bottom of the glove box, the distance along the vertical axis is 136 cm from the detector at the press quote and around 330 cm from the detector at the jar quote. Also, differently from the previous case, the shielding provided by the Kyowa glass reduces a lot the number of particles able to reach the detector. In particular, particles going in the direction coincident with the detector at the press quote must travel through a bigger portion of shield, since with an higher quote with respect to the source the angle of incidence of the particles with the Kyowa glass decreases and the length of the path inside the absorbing medium, in absence of scattering, is given by $l_{abs} = \delta_{Kyowa} \cdot \frac{1}{sin(\theta)}$, where δ_{Kyowa} is the thickness of the screen and θ the angle of incidence.

As in the previous case, gamma dose tends to saturate at high density values, but in this calculation the influence on the total dose is less important, since being outside the box neutrons, with a stronger penetrating power, play the major role.

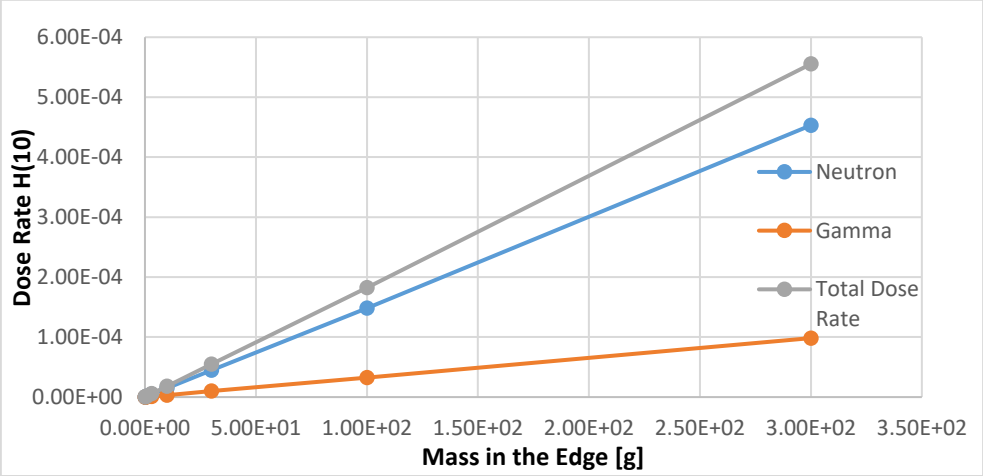

Figure 21: Homogeneous model, edge source with parametrical variation of the density, calculations outside the glove box at the press quote.

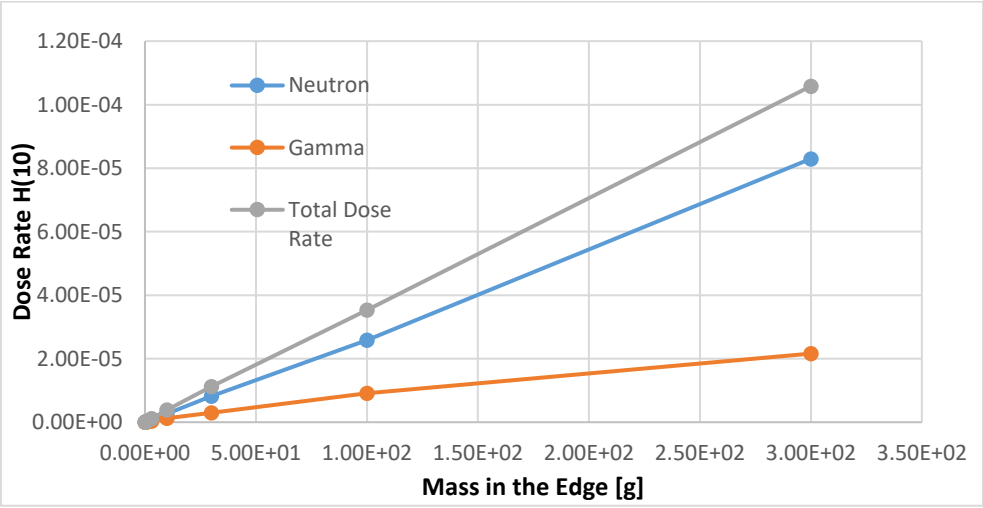

Figure 22: Homogeneous model, edge source with parametrical variation of the density, calculations outside the glove box at the jar quote.

Figure 21 shows the results of the edge simulations with the detector placed outside the glove box at the press quote, Figure 22 contains the results of the same analysis with the detector placed at the jar quote.

For the calculations concerning the edge source we can conclude with the same considerations of the corner case: here also, the distance between the source and the two detectors plus the shielding effect provided by the Kyowa glass reduce the dose equivalent rate. Since gamma rays are absorbed in great part, the smoother change in the slope of the dose curve is less evident than in the experiment with the detector placed inside the glove box.

Figure 23: Homogeneous model, Kyowa source with parametrical variation of the density, calculations outside the glove box at the press quote.

Figure 24: Homogeneous model, Kyowa source with parametrical variation of the density, calculations outside the glove box at the jar quote.

Figure 23 and Figure 24 show, respectively, the results of the Kyowa simulations with the detector placed outside the glove box at the press quote and at the jar quote.

Since this source is widely dispersed over the surface of the Kyowa glass, the effect of the different distance from the two detectors is less important. In fact, having a homogeneous flat emitter which covers a really large surface with the detection spots placed relatively far from the boundaries, the contribution will be more or less the same for both. More evident differences are given by the geometry of the glove box: in fact in the presence of the envelope of the jar there is a higher density of collision, and this may be the cause of scattering reactions leading to a slightly higher dose in that position. The behavior of the dose rate in function of the mass, instead, is absolutely the same found in the previous experiment: the reduced thickness of the source does not allow important absorption phenomena, so the problem collapses in a linear problem with direct dependence on the source intensity.

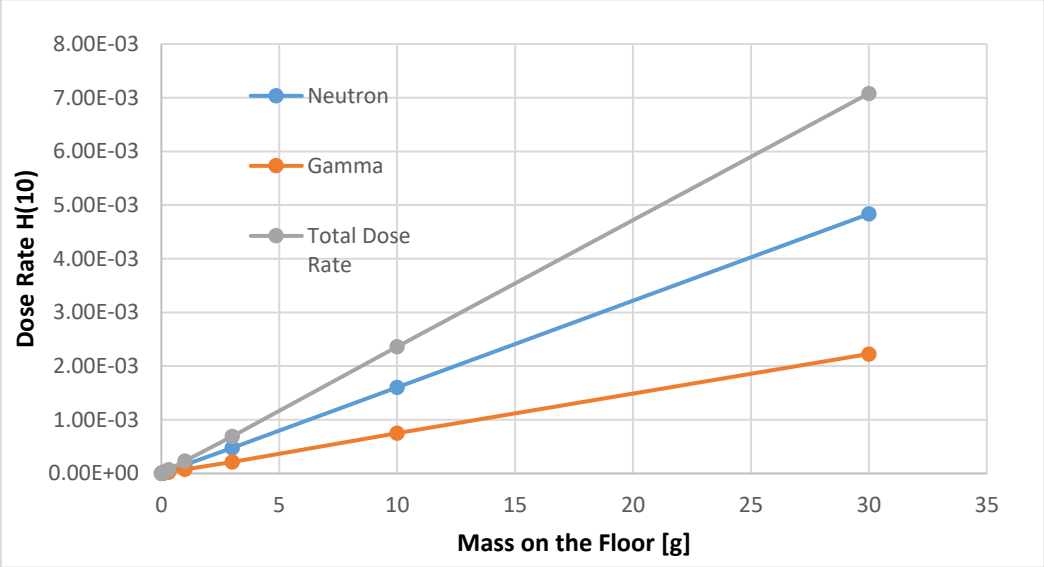

Figure 25: Homogeneous model, floor source with parametrical variation of the density, calculations outside the glove box at the press quote.

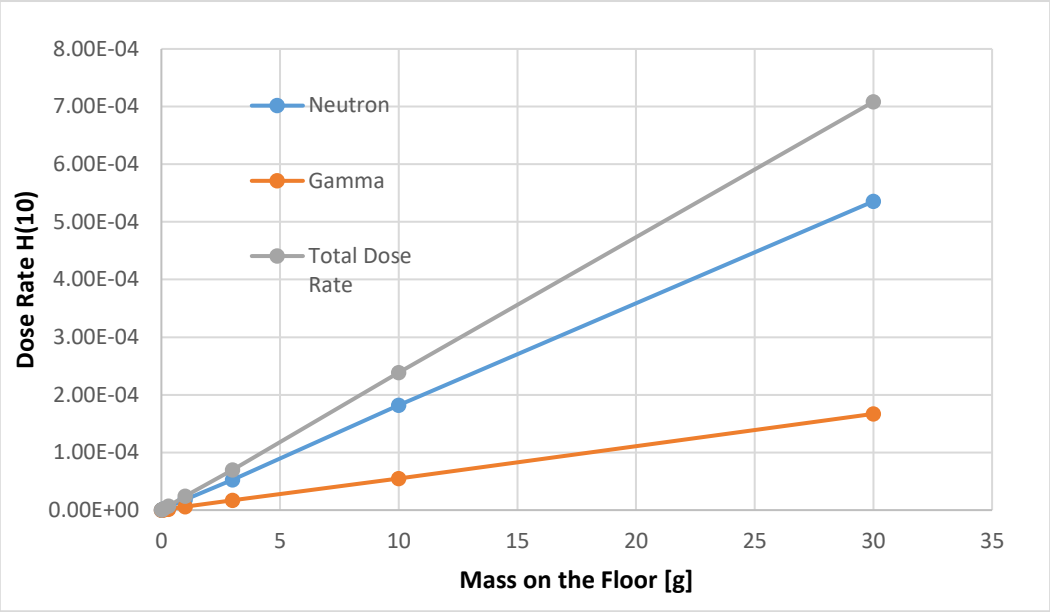

Figure 26: Homogeneous model, floor source with parametrical variation of the density, calculations outside the glove box at the jar quote.

Finally, Figure 25 and Figure 26 show, respectively, the results of the floor simulations with the detector placed outside the glove box at the press quote and at the jar quote.

With the floor source considerations from both the Kyowa glass source and corner source are valid: in fact, the behavior is the one typical of the flat, dispersed source, but thanks to the position with respect to the detectors there's a strong difference in the two calculations due to the increased distance.

The total dose equivalent rate calculated in each one of the previous cases and the PRSD of the simulations are reported in Table 7.

Table 7: Homogeneous model – Total dose equivalent rate and standard deviation.

	Mass [g]	Detector: External -Press		Detector : Internal		Detector : External - Jar	
		DED total	PRSD	DED total	PRSD	DED total	PRSD
Corners	1.00E-01	1.07E-05	1.54E+00	3.00E-01	3.00E-02	2.96E-06	3.17E+00
	3.00E-01	3.13E-05	1.56E+00	7.60E-01	3.08E-02	9.42E-06	3.99E+00
	1.00E+00	1.08E-04	1.73E+00	1.69E+00	3.71E-02	3.03E-05	3.33E+00
	3.00E+00	3.14E-04	1.75E+00	2.97E+00	5.02E-02	9.00E-05	4.26E+00
	1.00E+01	1.04E-03	1.72E+00	4.71E+00	1.50E-01	3.01E-04	3.12E+00
	3.00E+01	3.17E-03	1.72E+00	5.77E+00	9.43E-02	8.72E-04	3.29E+00
	1.00E+02	1.03E-02	1.70E+00	6.35E+00	1.58E-01	2.65E-03	3.58E+00
	3.00E+02	2.86E-02	1.56E+00	6.76E+00	3.30E-01	7.51E-03	3.55E+00

Edge	1.00E-01	1.84E-07	1.45E+00	7.03E-05	4.74E-01	3.89E-08	3.03E+00
	3.00E-01	5.50E-07	1.41E+00	2.09E-04	5.27E-01	1.13E-07	2.88E+00
	1.00E+00	1.85E-06	1.20E+00	3.77E-05	4.45E-01	3.70E-07	2.53E+00
	3.00E+00	5.51E-06	1.37E+00	1.13E-04	5.98E-01	1.16E-06	3.51E+00
	1.00E+01	1.83E-05	1.47E+00	5.94E-03	5.47E-01	3.88E-06	4.47E+00
	3.00E+01	5.47E-05	1.52E+00	1.39E-02	6.74E-01	1.13E-05	3.08E+00
	1.00E+02	1.82E-04	1.39E+00	2.97E-02	9.02E-01	3.53E-05	3.54E+00
	3.00E+02	5.55E-04	1.19E+00	5.21E-02	9.57E-01	1.06E-04	3.05E+00
Kyowa	1.00E-02	1.17E-05	2.68E+00	4.89E-02	9.73E-02	1.28E-05	3.07E+00
	3.00E-02	3.57E-05	2.30E+00	1.47E-01	9.73E-02	3.54E-05	2.49E+00
	1.00E-01	1.20E-04	2.80E+00	4.89E-01	9.73E-02	1.20E-04	2.52E+00
	3.00E-01	3.55E-04	2.86E+00	1.47E+00	9.73E-02	3.74E-04	2.90E+00
	1.00E+00	1.17E-03	2.58E+00	4.89E+00	9.73E-02	1.21E-03	2.71E+00
	3.00E+00	3.70E-03	3.01E+00	1.47E+01	9.73E-02	3.52E-03	2.69E+00
	1.00E+01	1.24E-02	2.80E+00	4.89E+01	9.73E-02	1.25E-02	2.64E+00
	3.00E+01	3.57E-02	2.79E+00	1.47E+02	9.73E-02	3.77E-02	2.81E+00
Floor	1.00E-02	2.29E-06	1.02E+00	1.98E-05	7.85E-01	2.43E-07	3.06E+00
	3.00E-02	6.94E-06	1.01E+00	5.90E-05	5.23E-01	7.18E-07	2.98E+00
	1.00E-01	2.31E-05	9.48E-01	1.96E-04	5.69E-01	2.44E-06	2.98E+00
	3.00E-01	6.97E-05	1.03E+00	5.86E-04	5.12E-01	7.03E-06	2.80E+00
	1.00E+00	2.31E-04	1.03E+00	1.96E-03	5.44E-01	2.44E-05	2.93E+00
	3.00E+00	6.90E-04	1.07E+00	5.86E-03	5.04E-01	6.98E-05	2.76E+00
	1.00E+01	2.36E-03	1.39E+00	1.95E-02	5.84E-01	2.39E-04	2.77E+00
	3.00E+01	7.08E-03	1.07E+00	5.86E-02	1.08E+00	7.08E-04	2.66E+00

4.2.2 Parametrical Variation of the Source Thickness

This analysis has the aim to better investigate the effect of self-shielding of the source that was clearly visible on the gamma ray dose equivalent rate curve in the previous analysis. To better study this phenomenon, the position of the detector has been changed: the calculations are made at a distance of 15 centimeters from the center of the source. This makes easier the convergence of the simulations, since with a reduced distance the number of sampling increases a lot.

To make a comparison with further results, the parametrical analysis on the mass density of the corner source with calculations using the new detector was carried out:

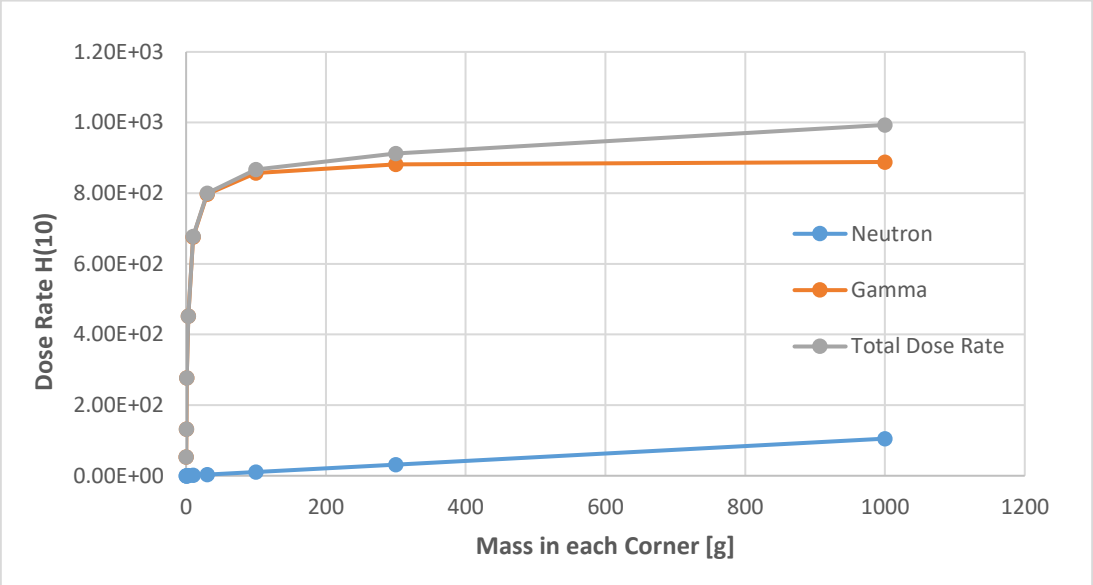

Figure 27: Homogeneous model, corner source with parametrical variation of the density, calculations at 15 cm from the source.

From this calculation, made immediately next to the source, it is clearly visible in Figure 27 that after a critical value of density the dose due to gamma rays becomes constant, while neutron dose continue to behave linearly. The same detector position will be used for the experiment with constant density and variable thickness, but even for comparisons with stochastic geometries, because it makes possible to have a clear idea of the source behavior and it makes also the simulation converges more easily.

The first experiment has been made considering a mass density of the source of $0.08\frac{g}{cm^3}$, corresponding to a mass of 10 g of radioactive dust in the previous experiments. The source is then "divided" in 50 slices of 1 mm thickness and 5 cm of base side. Those slices are added one by one, starting from the one immediately next to the detector going back, until the entire cube is filled completely by the source material (naturally, this result will coincide with the 10 gram simulation with the previous system). The results of the experiment are reported in Figure 28.

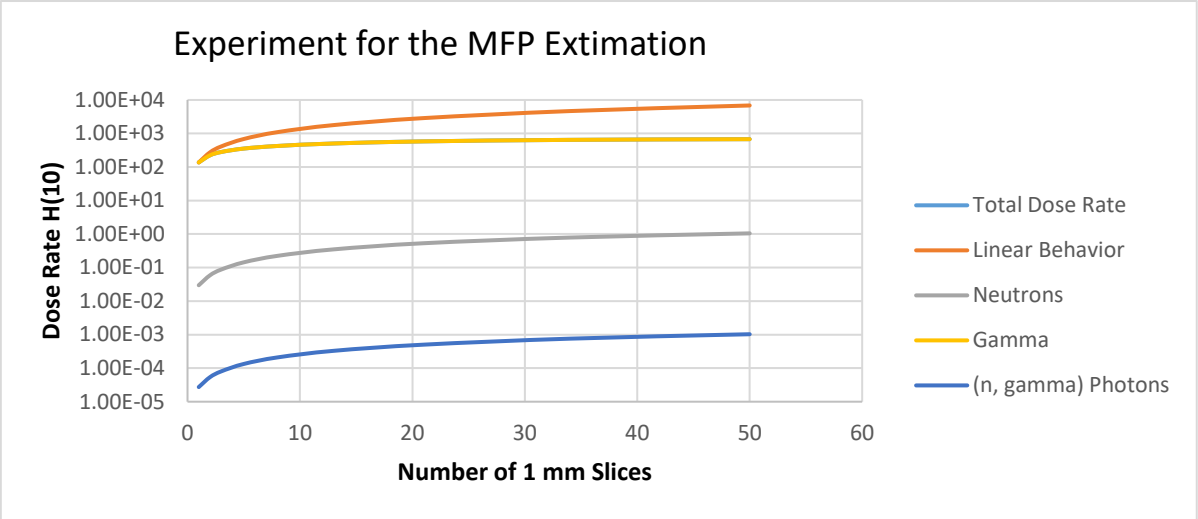

Figure 28: Homogeneous model. 1mm slices with density 0.08 g/cm3 added progressively in the corner of the glove box. Calculations made at 15 cm from the center of the cube.

The plot in Figure 28 is in logarithmic scale to better show the difference between each particle: gamma rays are the principal contributors to the dose equivalent rate, and the dose provided by them becomes practically constant after less than 2 centimeters of thickness. Neutrons behave practically linear, but their contribution is way smaller. The conclusion is that, again, the penetrating power of gamma particles in the source medium itself is way smaller than the neutron penetrating power.

It is possible to show that variating the absorption cross section of the single slice, so variating the density, the saturation effect increase with the increase of the cross section and vice versa.

Figure 29 represent the dose equivalent rate H(10) measured with the same procedure, but with a mass density of the slices equal to 0.008 g/cm^3.

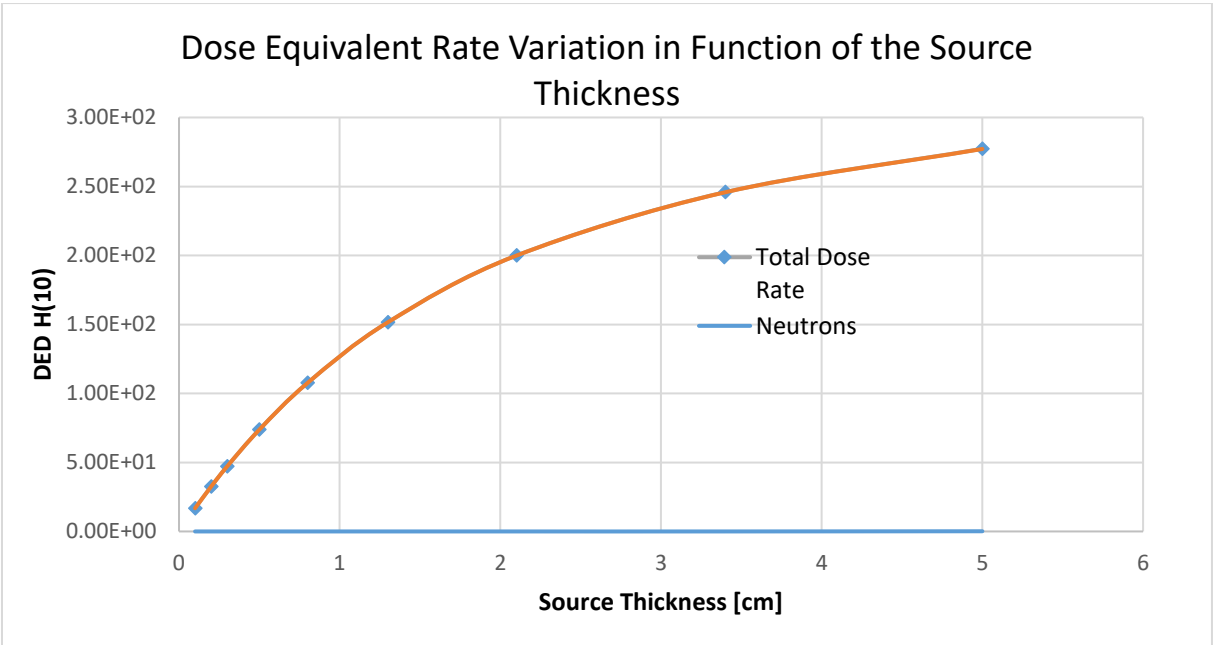

Figure 29: Homogeneous model, corner source with parametrical thickness variation at a fixed density of 0.008g/cm^3.

To make the same experiment with an higher density, it was necessary to decrease the thickness of the slices from $1mm$ to $50\ \mu m$, since a layer of one millimeter was already sufficient to shield completely gamma rays coming from the inside of the source. The results are shown in Figure 30.

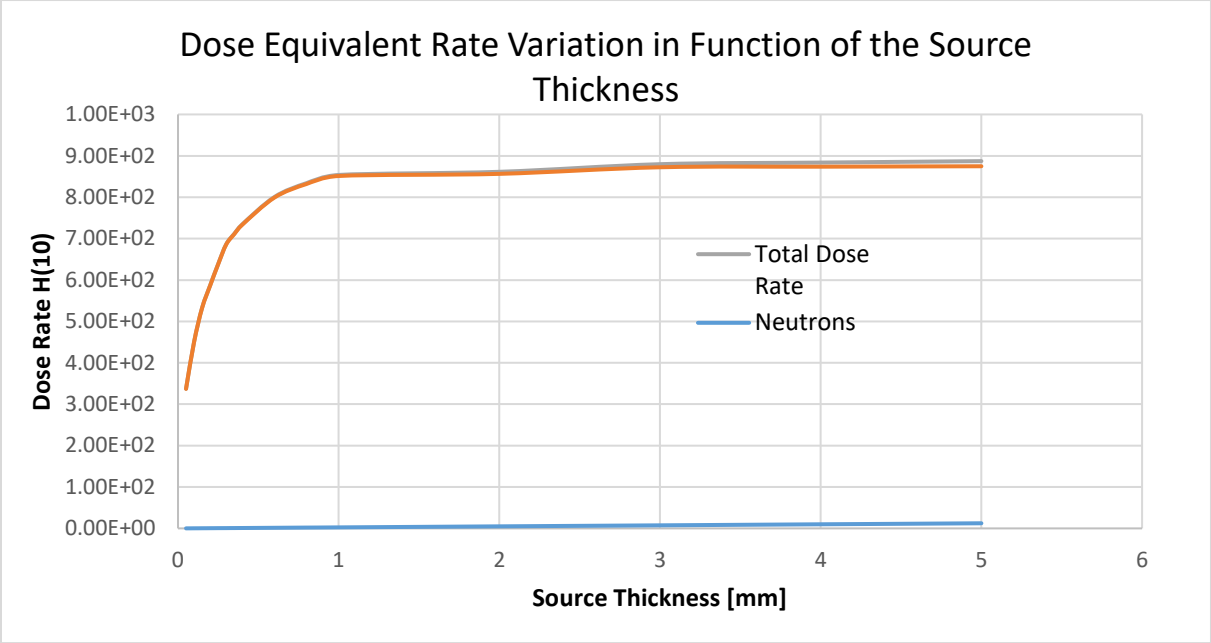

Figure 30: Homogeneous model, corner source with parametrical thickness variation at a fixed density of 6.6 g/cm^3.

The aim of the experiment is to get an idea of the magnitude of the mean free path of neutrons and gamma rays. Results show that in a dispersed medium, the thickening of the source does not lead to an immediate saturation, while in a compact medium the saturation occurs after less than $1mm$. Considering the transport equation for the source problem:

$$\Phi(\vec{r}, E, \vec{\Omega}) = \frac{1}{4\pi\|r - r'\|}\int_0^s ds' S(\vec{r'}, E) exp\left[\int_0^{s'} ds'' \Sigma(E)\right] \tag{58}$$

it is clear that the integral of the optical path length in an homogeneous medium depends on the product between the portion of traversed material and its cross section. In practice, there is a common effect involving both factors, and that is clearly visible in case of the parametrical variation of density on the Kyowa glass, where there aren't appreciable effects due to the density changes because of the very low thickness.

4.2.3 Discrete Homogeneous Model

The first test with the discrete homogeneous model is done using a 10·10 mesh on the Kyowa glass. The results of this test are shown in Figure 31. The density in each cell could variate, according to a uniform probability density function, in the interval $[0.9 \cdot \bar{\rho}\,; 1.1 \cdot \bar{\rho}]$. Here are reported the results of 10 different simulations, so 10 different mass dispersions on the Kyowa glass. Simulations for gamma rays are done by using 100000 batches of 5000 particles each, for an average accuracy of 0.87%.

This relative error corresponds to about 0.425 $\mu Sv/h$ in absolute value, so it can be noticed that in some cases the discrepancy between the results is slightly bigger than the confidence interval.

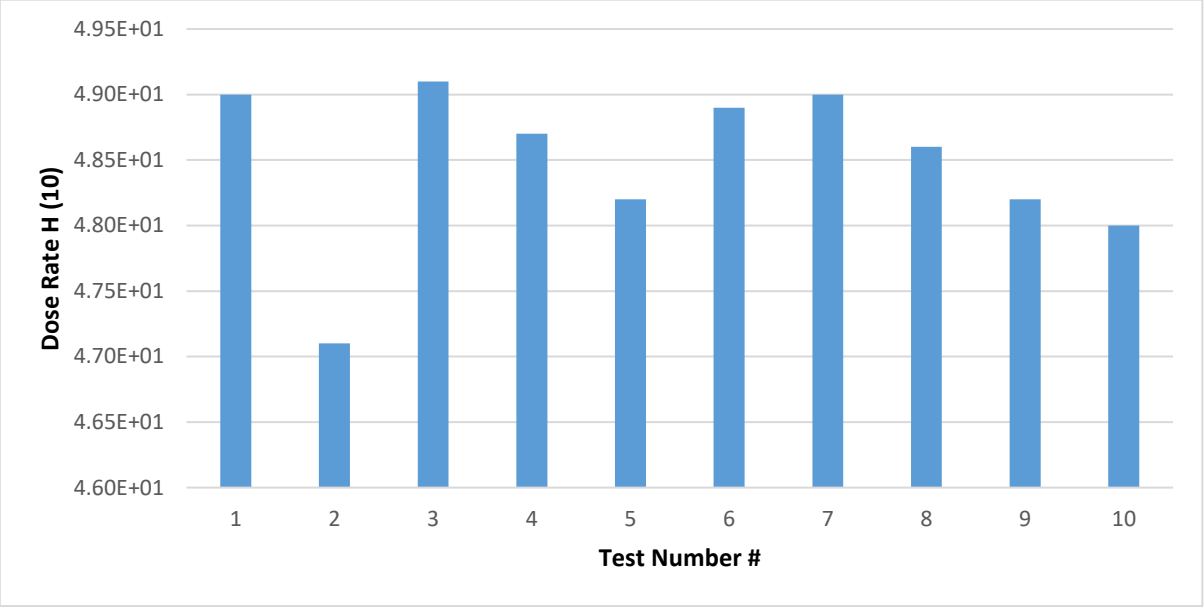

Figure 31: Discrete homogeneous model applied on the Kyowa surface. Simulations with 10 grams of total mass. Gamma dose rate calculated above the press. Average PRSD of the simulations: PRSD=0.87.

For what concerns neutrons, results are reported in Figure 32 for the sake of completeness, even if the discrepancy between the results is smaller than the relative error of the single simulation.

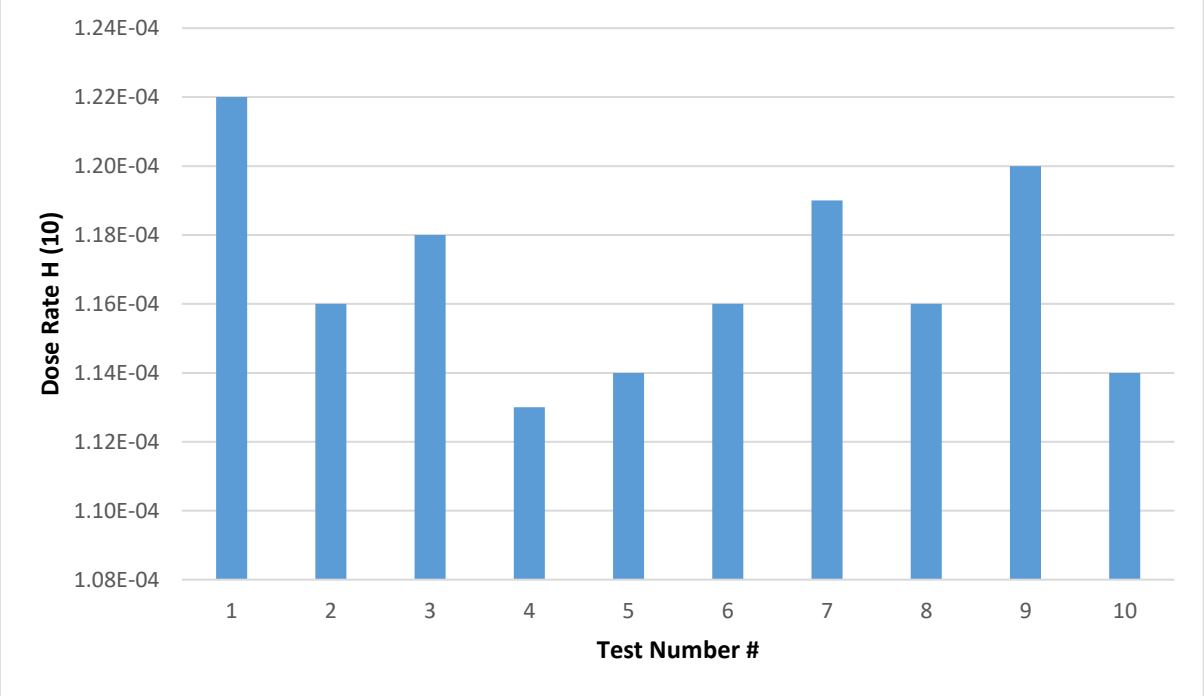

Figure 32: Discrete Homogeneous Model applied on the Kyowa surface. Simulations with 10 grams of total mass. Neutron dose rate calculated above the press. Average PRSD of the simulations: PRSD = 3.4.

The average PRSD for the simulations, where 10000 batches of 3000 particles each one were used, is around 3.4%. Thus the interval of confidence is way bigger than in the previous case.

We can conclude saying that the discrepancy between the output results is way smaller than the discrepancy between the source intensities of different cells of the mesh. Naturally, with a relatively large size of the single cell, the output results are strongly influenced by the concentration of radioactive material in the cells immediately next to the detectors. To highlight this aspect, the following experiment was carried out: the mass is intentionally concentrated in the center of the surface, and the dose rate measured increases as the mass gradient along the surface increases. This is done, as explained in section 2.2.3, distributing the mass with a density function which is the joint function of two normal distributions. Variating the σ term in the equations, the concentration gradient can be changed, leaving constant the total amount of mass on the whole surface. Figure 33, Figure 34 and Figure 35 show, respectively, the gamma dose equivalent rate in function of the variance of the distribution calculated outside the box at the press quote, inside the box at the press quote and outside the box at the jar quote. Figure 36, Figure 37 and Figure 38 show, respectively, the neutron dose equivalent rate in function of the variance of the distribution calculated outside the box at the press quote, inside the box at the press quote and outside the box at the jar quote. It is possible to notice that the dose equivalent rate is higher with a smaller σ (the variance term of the normal distribution represents the dispersion of the curve, so a small σ corresponds to a narrow bell curve and vice versa).

1. Gamma dose equivalent rate:

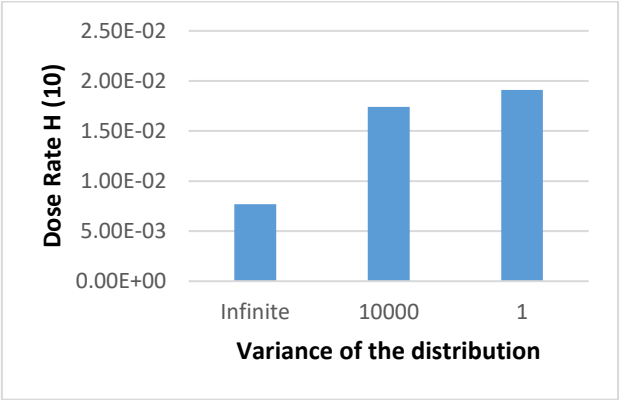

Figure 33: Variation of the dose equivalent rate H (10) in function of the dispersion of the density distribution. Calculations done outside the box, at press quote.

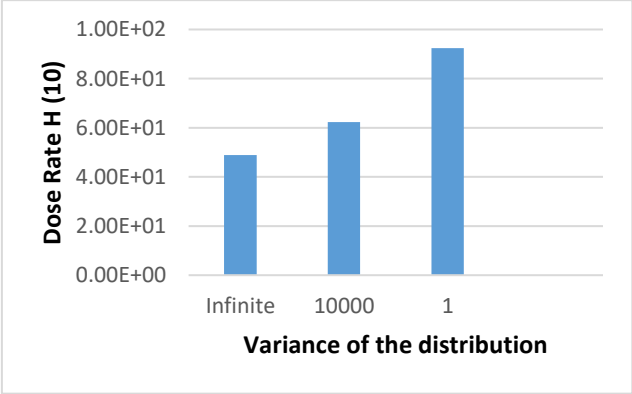

Figure 34: Variation of the dose equivalent rate H (10) in function of the dispersion of the density distribution. Calculations done inside the box, at press quote.

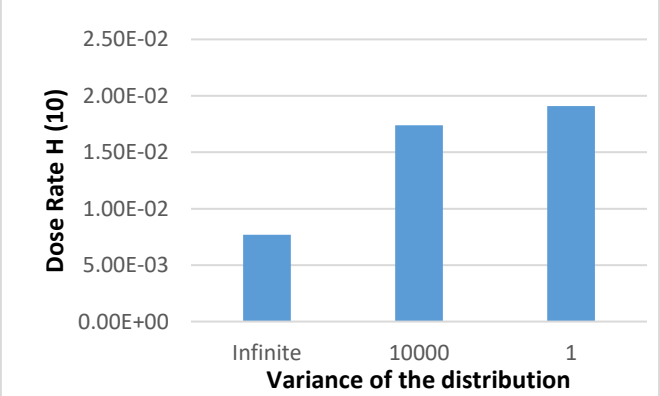

Figure 35: Variation of the dose equivalent rate H (10) in function of the dispersion of the density distribution. Calculations done outside the box, at jar quote.

2. Neutron dose equivalent rate:

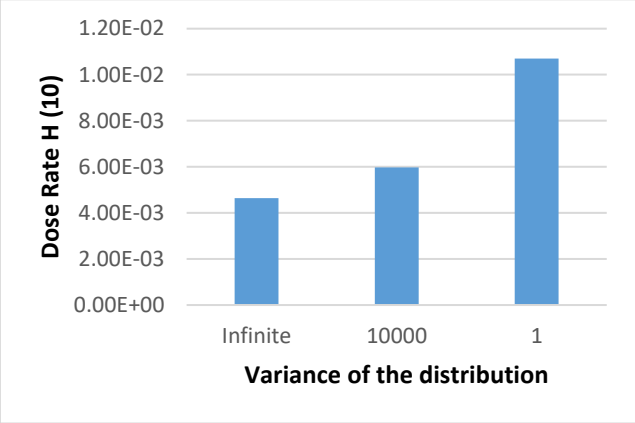

Figure 36: Variation of the dose equivalent rate H (10) in function of the dispersion of the density distribution. Calculations done outside the box, at press quote.

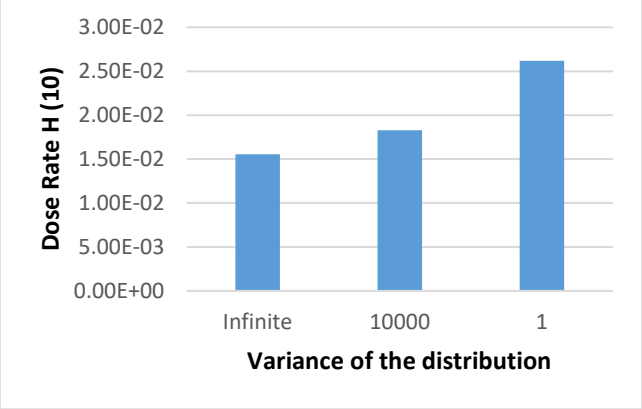

Figure 37: Variation of the dose equivalent rate H (10) in function of the dispersion of the density distribution. Calculations done inside the box, at press quote.

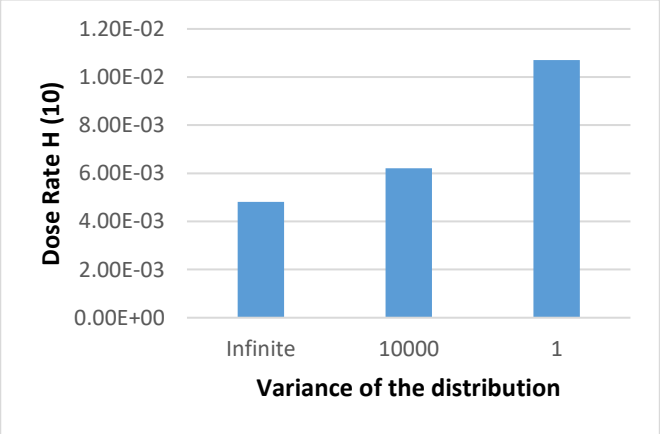

Figure 38: Variation of dose equivalent rate H (10) in function of the dispersion of the density distribution. Calculations done outside the box, at jar quote.

4.3 Monodispersed Radius Spherical Inclusions Methods

As mentioned before, in this kind of experiment the source is composed of a set of very small volumes, instead of a single larger one. Since this source geometry is obtained with a stochastic algorithm, is important to check if different spatial dispositions of the spheres could give different output results with the same control volume V, packing fraction ξ, radius and the density of the spheres. For the sake of simplicity, this test was carried out considering one of the two volumes used in the homogeneous model to simulate the dust accumulated in the corner of the box as control volume, since the in following experiments the inclusions are generated in that position. The density of the spheres is equal to $\rho_{MOX} = 6.6 g/cm^3$.

The mass simulated in the control volume is equal to $1g$, which corresponds to a packing fraction of $\xi = 0.00121$ and a number of spheres $N = 287$, if a radius of half a millimeter is used. The results of the analysis are shown in Figure 39.

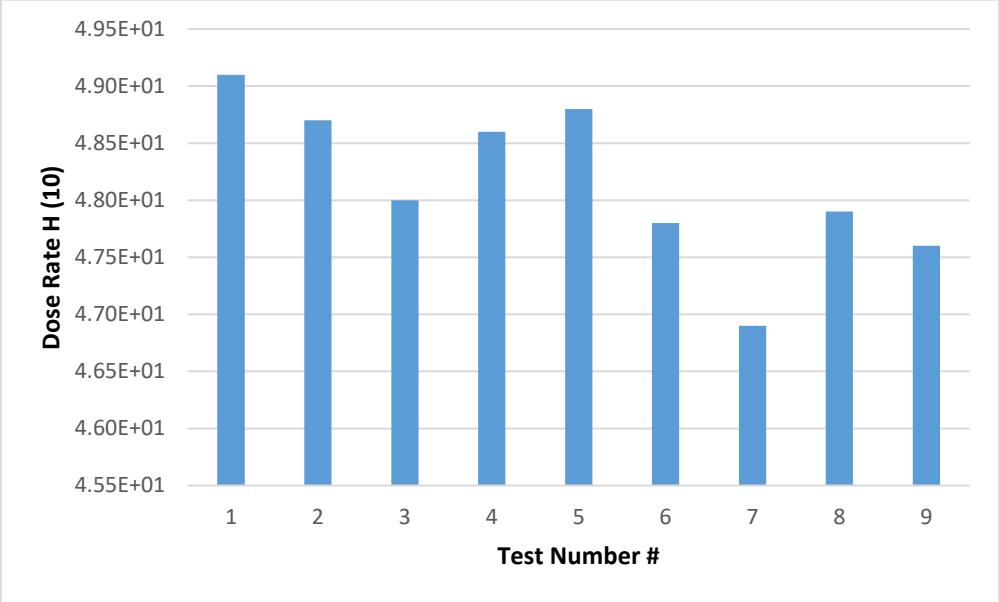

Figure 39: Comparison between 9 realizations of monodispersed radius spherical inclusions with R = 0.05 cm, $\xi = 0.00121$ and $\rho_{MOX} = 6.6 g/cm^3$.Spheres with MOX composition inside an air matrix. Gamma dose calculated at 15 cm from the center of the source. The PRSD of each Monte Carlo simulation is below 1%, for an average PRSD of 0.95%.

In these simulations 1000 batches of 5000 particles each one are used, for an average PRSD of ~0.95%. Results show that the discrepancy between different realizations is not wider than the interval of confidence of the simulations output.

Things change for example, doing the same experiment with an inclusion generated inside a metallic matrix instead of an air matrix:

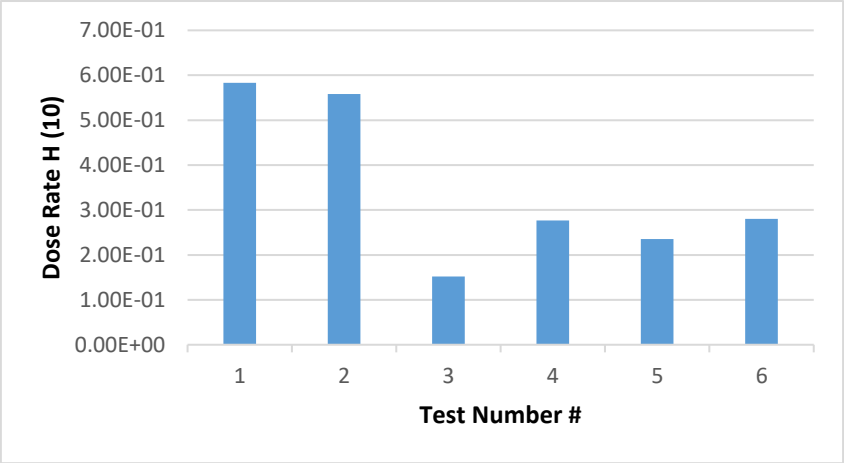

Figure 40: Comparison between 9 realizations of monodispersed radius spherical inclusions with R = 0.05 cm, ξ=0.00121 and ρ_MOX=6.6g/cm³.Spheres with MOX composition inside an uranium matrix. Gamma dose calculated at 15 cm from the center of the source. PRSD of the results is below 5%.

In this experiment, whose results are shown in Figure 40, the matrix of the spherical inclusion is a uranium 238 matrix, and in the calculation only particle emitted by the spheres are simulated. The discrepancy of the simulations in this case is very high, and the reason for that is the shortening of the mean free path of gamma rays in the matrix, that gives importance to the starting point of the emitted particle, and so to the position of the emitter. In an air matrix, the most important phenomenon is the self-shielding of the spheres themselves, but once the particle escapes from the source, it is almost free to travel (the density of the inclusion is really small).

In the following calculations, since an air matrix is used each time and the discrepancy between different simulations never reaches values above the double of the standard deviation of the Monte Carlo simulation, only one result for each set of parameters (ρ, ξ, R) will be reported.

4.3.1 Parametrical Analysis – Variation of the Radius of the Spheres

Using the RSA method allows us to act on the source thickness without changing density and mass. In this case the only thing that changes is the portion of source material that the particles must traverse to get out from the source itself. A smaller diameter of the emitter leads to a bigger leakage from the sphere boundary, with a consequent increase of the global dose rate. In a convex geometry containing a monodispersed radius inclusion, the expression of the average chord length becomes: $\Lambda_0 = \left(\frac{1}{\xi} - 1\right)\frac{4}{3}r$ [31].

In this case the global max is fixed to $1\ g$, thus the packing fraction is also fixed to the value $\xi = 0.00121$. In this experiment, simulations with really small radius are not trivial to carry out: to simulate one gram of dust using spheres with $d = 100\mu m$, the number of volumes reaches almost 300000. This naturally leads to a very long computational time, even after the acceleration methods described in section 3.6.

Each simulation was done with a different geometrical disposition of the spheres, obtained with the RSA method and properly processed by Python scripts to be inserted into the corners of the glove box. Naturally, as said in the section 3, each sphere will represent an independent source. A few batches of 5000 particles are necessary to obtain a good accuracy: the simulations never pass the 100 batches, and the accuracy obtained is below 4% of PRSD for each case.

To study particles smaller than $50\mu m$ it was necessary to reduce the total amount of mass, so the packing fraction. This because the maximum number of volume the code is capable to simulate is 1000000, and to simulate one gram of dust using spheres with a diameter of $50\mu m$ implies the utilization of more than 1100000 volumes. The results of the parametrical analysis are shown in Figure 41 and Table 8.

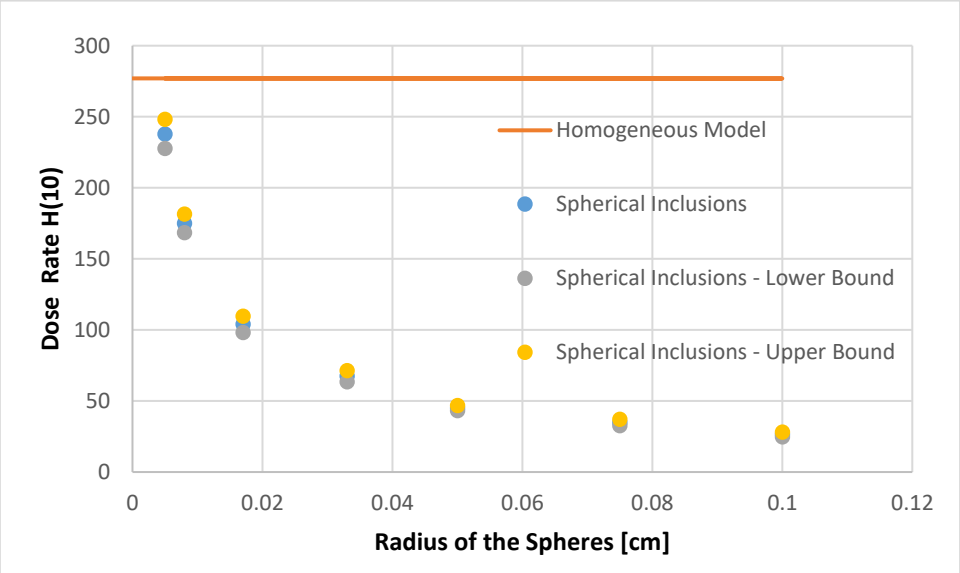

Figure 41: RSA spherical inclusion method, gamma simulations with different values of the spheres radius with a constant mass of 1g for each corner and constant density of 6.6 g/cm^3. PRSD of the results is reported in Table 8. Lower Bound and Upper Bound are obtained using twice the PRSD as relative error.

It is interesting to notice that, since the radius of the spheres is directly proportional to the average chord length of the geometry, having a small radius means getting closer to the atomic mix: in fact the results with small spheres are really close to the one obtained using the homogeneous model. The behavior of the curve in function of the radius is nearly exponential: this makes sense, since the attenuation of the radiation flux inside an absorbing medium follows an exponential law. Since the average chord length of the spheres increases linearly with the increase of the radius, and since the average chord length is, by definition, the mean portion of matter that a particle traveling following a straight line will meet during its flight, it is logical to treat the increase of this quantity as the increase of the thickness of an absorbing medium each particle has to go through. Going backwards with the radius value, the portion of solid material traversed by each particle will be smaller and smaller, until a singularity will be reached, so when the emitters are punctual. This is naturally physically impossible, but the behavior of the dose curve (it was impossible to simulate smaller particles due to the limits of the software) shows the possibility of a vertical asymptote in proximity of the 0 diameter.

Luckily, emitters with no thickness and no cross section are impossible to find, so it can be logic to assume that the superior limit for the results with small spheres using stochastic spherical inclusions is exactly the result of the homogeneous model.

Table 8: Monodispersed radius spherical inclusions – Simulation parameters and standard deviation.

Sphere Radius [cm]	PRSD	Dose Rate H (10)	# of spheres	Batch Time	Data Reading Time
0.1	3.21E+00	2.65E+01	36	<1s	1s
0.075	3.25E+00	3.49E+01	85	<1s	2s
0.05	2.02E+00	4.51E+01	287	1s	16s
0.033	2.89E+00	6.75E+01	998	8s	63s
0.017	2.80E+00	1.04E+02	7302	110s	6624s
0.008	1.86E+00	1.75E+02	70068	~1200s	N.D.
0.005	2.16E+00	2.38E+02	287372	>10000s	N.D.

4.3.2 Parametrical Analysis – Variation of the Packing Fraction

Since the packing fraction of the spherical inclusions is, instead, inversely proportional to the average chord length of the matrix, increasing the global mass of the source maintaining constant the density and the radius of the spheres will lead again to a convergence with the homogeneous case. The procedure for the simulation is the same, and the issues are similar: in fact, having a great amount of mass means having a huge number of spheres. In this case, the maximum number of spheres is smaller than the previous analysis (10 times less), and this made the analysis faster and easier.

Here the radius of the spheres is fixed to $R = 0.05\ cm$, the density to $\rho_{MOX} = 6.6 g/cm^3$ and the packing fraction varies from 0.000121 to 0.121. Naturally, having a huge packing fraction makes the model more similar to a homogeneous system, in a similar way of reducing the radius of the spheres. What happens in the analysis is that the probability for a particle of impacting another sphere while traveling increases with the increase of the packing fraction, so the dose equivalent rate curve, initially straight, begins to saturate at around 10 grams of dust simulated.

Results are shown in Figure 42. It has to be noticed that initially the slope of the curve is higher than in the curve for the homogeneous model: in fact the dose equivalent rate measured in this experiment, initially way smaller than the value obtained with the homogeneous model, converges with this last one at high packing fractions.

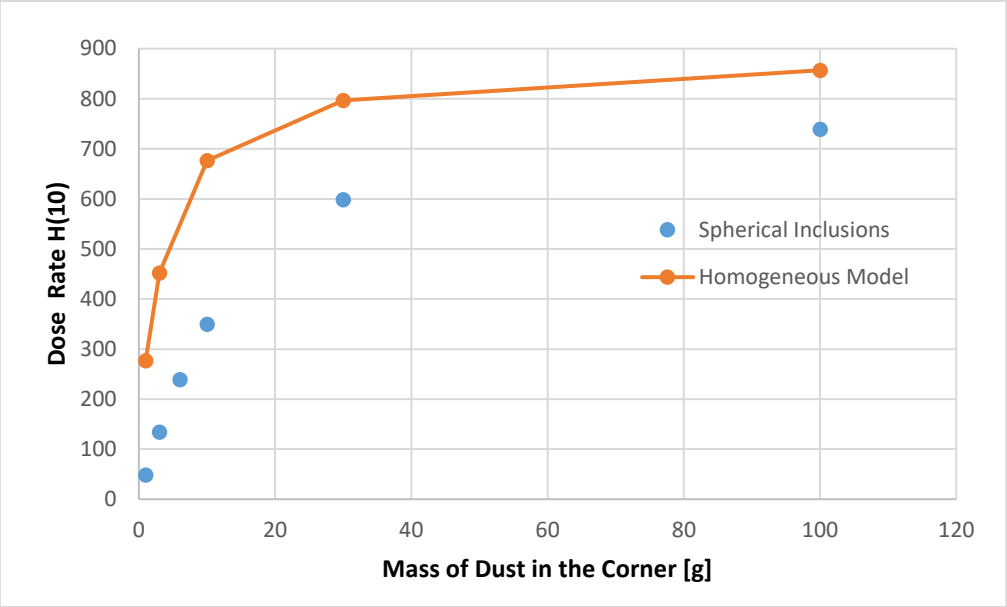

Figure 42: Spherical inclusion model, gamma simulation with spheres with a fixed constant radius of 0.5 mm and a constant density of 6.6g/cm3 with variable packing fraction. Simulations are stopped when the PRSD is below 2%.

4.3.3 Neutron Simulations with Spherical Inclusions

While gamma rays have a mean free path comparable to the characteristic dimensions of the simulated medium, neutrons have a mean free path that is much longer. The difference between the neutron dose equivalent rate coming from a source simulated using a stochastic geometry of any kind and one simulated using an homogeneous volume is smaller than the standard deviation of the TRIPOLI-4® results. In the following plots are reporting the results of a neutron simulation using the RSA method. Each value of mass is simulated with 5 different dispositions of the spheres, so 5 different RSA realizations. All the simulations are done using 200 Batch of 3000 particles each one, for an accuracy of $PRSD \sim 2.5\%$. A comparison between the results of this simulation and the results of the homogeneous model is shown in Figure 43. The smallness of the error band is visible looking at the small discrepancy between different simulations.

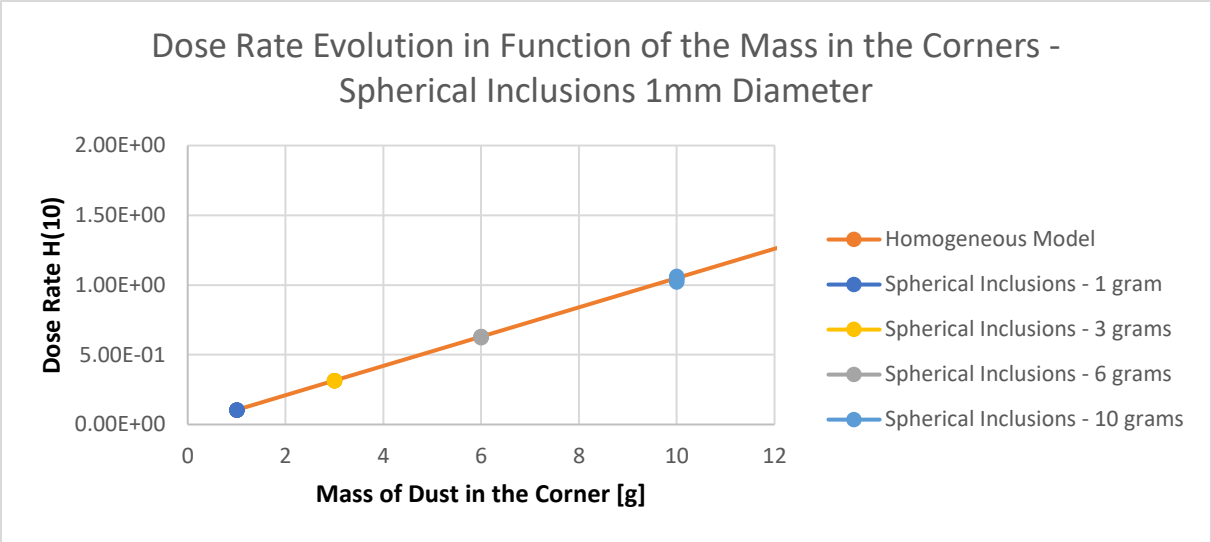

Figure 43: Spherical inclusion model, neutron simulation with spheres with a fixed constant radius of 0.5 mm and a constant density of 6.6g/cm³ with variable packing fraction. The PRSD of the spherical inclusion simulations is ∼2.5%.

The results coming from the homogeneous model fall exactly in the middle of the confidence interval of the RSA simulations. For the sake of simplicity, only this plot is reported, since apparently there is no benefit for this kind of particle to use a sophisticated geometry instead of a simple one. This is an example of how the atomic mix (see Eq. (24) in section 2.1.5) influences the results: the experiment with the thickness variation using the Homogeneous Model (section 4.2) showed that the mean free path of the neutrons has a length scale way bigger than the dimension of the source, so the chunks of the binary matrix that a flying neutron is able to "see" during its path can be huge. This leads to a behavior of the neutron flux and so of the dose equivalent rate very similar to what can be found in the homogeneous case.

4.4 Other Stochastic Geometries

Another important aspect, due to the short mean free path of the gamma rays, is the magnitude of the external surface of the source. It can be shown that for particles facing directly the environment, the superposition of the effect is applicable. In fact, since no absorption occurs in the flight direction because of other spheres, the dose measured in the detector is simply the dose coming from one single sphere multiplied by the number of spheres.

This analysis has a different meaning with respect to the previous parametrical analysis: the aim is not to show a convergence with the homogeneous case, but just to analyze the effect of different spatial distribution of the same mass of dust. Having different dispositions means changing the mean distance of the particles from the detector, having a different, non-uniform

packing fraction and having a chord length distribution that can change a lot from the simple cubic case.

Anyway, it will be showed that different dispositions could give output results bigger than the ones obtained with the simple RSA method, but always smaller than the homogeneous model results.

In the following plots are reported the results of different geometrical shapes, always contained in the original control volume, with fixed mass, density and diameter of the spheres.

All the geometries are created without the RSA algorithm, but with the one explained in section 3.4. Four geometrical shapes are proposed: two of them, the ones obtained by the intersection of the cube with a sphere octant and with three hyperbolic cylinders, aim at simulating a situation in which the dust is accumulated in the edges of the cube. The "Sheet" shaped geometries aim at maximizing the number of spheres on the surface immediately exposed to the external environment. Two configurations of sheet-shaped geometry are proposed: one placed on the face of the cube immediately next to the detector, and another on the back face of the cube (so the farthest face of the cube with respect to the detector). All the geometries are composed by 289 spheres of $1mm$ diameter and $\rho = 6.6\ g/cm^3$, for a total mass of $1g$. Naturally in this case the packing fraction of the geometry changes case by case, so does the average chord length, and the comparison with the homogeneous model is not as trivial as before. Indeed the dispersion of spheres is no longer uniform and isotropic. Naturally, the geometry with the highest packing fraction is the Sheet-Shaped, followed by the ones obtained with, respectively, the hyperbolic cylinders and the sphere octant. To compare the two algorithms for spherical inclusion, in the end, a cubic geometry is proposed, with dimension analogue to the RSA simulations. Is interesting here to notice that the same shape of the disposition (the cubic one) with the same parameters of the spheres but a different generation algorithm gives, in practice, the same dose equivalent rate value. All the simulations are done using 1000 Batch of 5000 particles each one, for an accuracy of PRSD < 1% in each case.

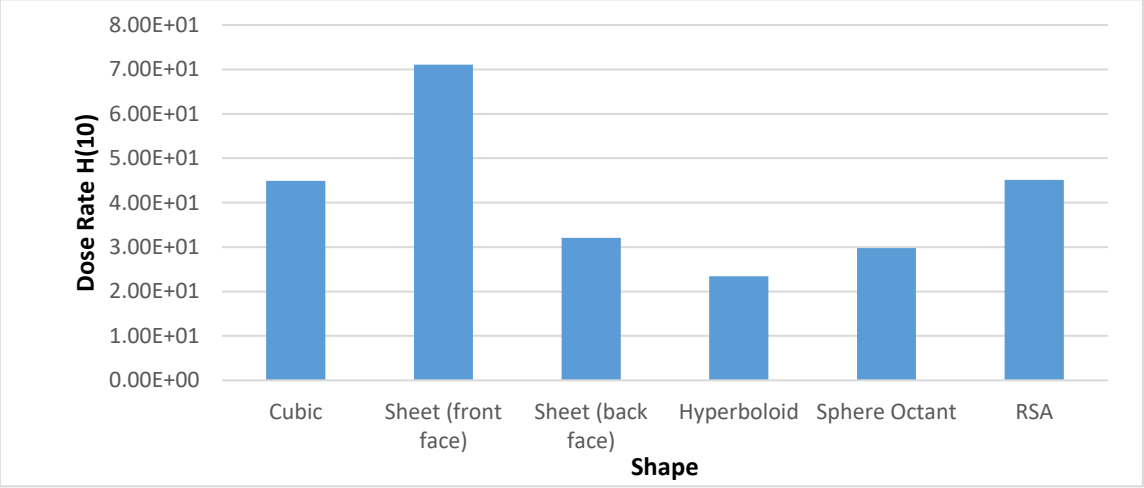

Figure 44: Comparison between the dose rate obtained with different geometrical configuration, at constant mass of 1g and density = 6.6 g/cm^3. The detection point is at 15 cm from the center of the original cubic source. PRSD of the simulations < 1%.

The results, shown in Figure 44, are strongly influenced by the shape at a local scale: the effect of the shape variation becomes less and less important with the increase of the distance of the

detection spot. This is due to the effect of the distance of the single sphere, which can be very important using a detector with a distance of 15 centimeters from the center of the original cubic source (for example, the two Sheet-shaped geometries are identical; only the distance from the detector changes). If the test is repeated using as detection spot the point just above the press used in the first analysis, the results will not differ a lot. Simulations in this case are more complicate (achieving a good accuracy with spherical inclusions using a detector far from the source requires a very long computation time), in fact the average accuracy is around PRSD = 5%. The results of the test are shown in Figure 45.

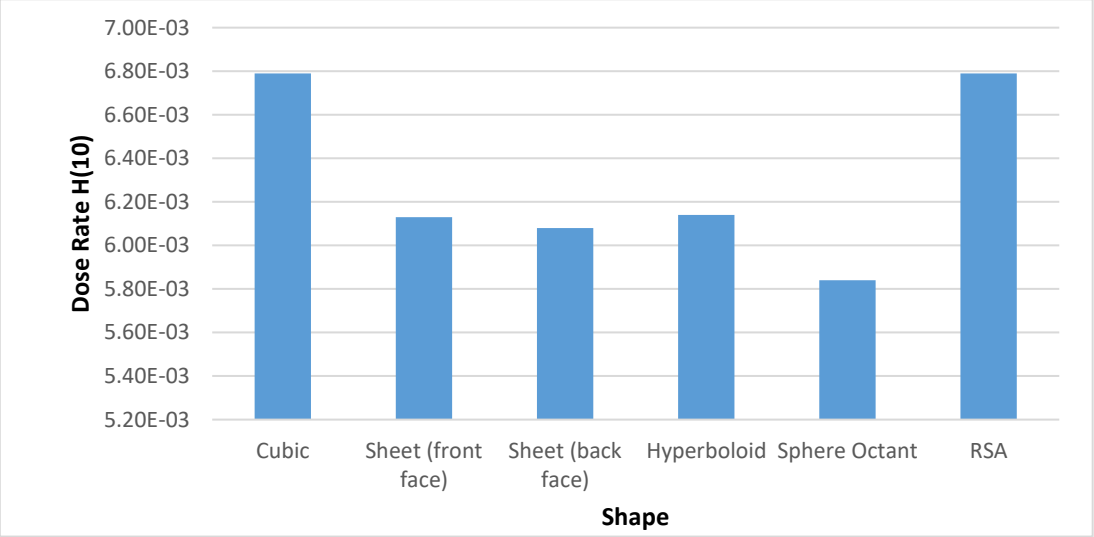

Figure 45: Comparison between the dose rate obtained with different geometrical configuration, at constant mass of 1g and density = 6.6 g/cm^3. The detection point is above the Press. PRSD of the simulations $\sim 5\%$.

4.5 Dust Aggregates Simulation

With the simple spherical inclusion method it is possible to see the difference between a homogenized system and a dispersed system. However, dust aggregates are taken as homogeneous spheres. It is impossible, due to the complexity of the situation to simulate exactly the shape of a dust aggregate, but it is possible to see the difference between a single volume with averaged properties and an aggregate of dense volumes in an air matrix with this kind of simulation. These simulation were carried out considering each ensemble of 12 spheres as an independent source. For problems related to the TRIPOLI-4® code, it was impossible to use acceleration methods used in sections 4.3 and 4.4, thus the analysis is done for small values of mass. 1000 Batches of 5000 particles were more than sufficient to obtain a good accuracy, below the 1% ($PRSD < 1\%$).

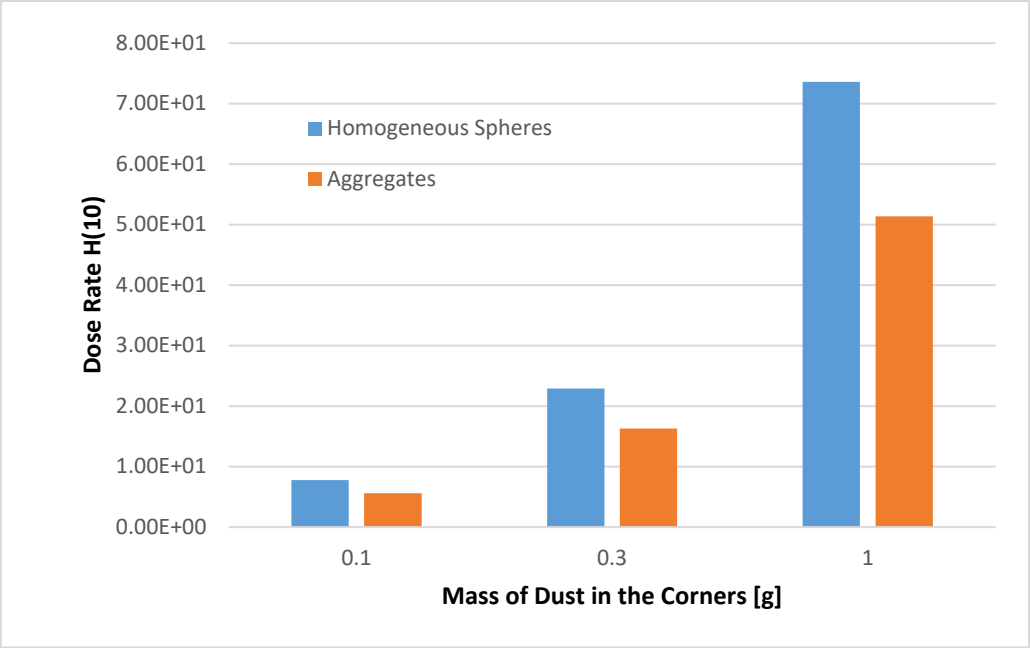

Figure 46: Comparison between gamma dose equivalent rate obtained with an inclusion of homogeneous spheres and an inclusion of dense packing of 12 spheres inside a sphere of the same radius as the homogeneous one. PRSD of the aggregates simulations < 1%.

Figure 46 shows the comparison between the gamma dose equivalent rate calculated using dense packings of 12 spheres (orange) and the dose rate calculated using homogeneous spheres with the same radius and the same mass of the 12 spheres aggregate.

The simulation is done considering the exact density value of the MOX fuel for the small spheres, equal to $\rho_{MOX} = 11.016 g/cm^3$, composing the dense packing, and a density equal to the average one of the packing , so equal to $\rho_{MOX} \cdot \xi_{12-packing} = 4.67 g/cm^3$, for the homogeneous ones. The dose changes in the way it changed passing from the homogeneous cube to the spherical inclusion: instead of a single emitter with a low density there are several with a higher one, and this leads to an increase of the self-shielding of the sources, and so a decrease of the dose equivalent rate measured.

4.6 Poly-Dispersed Radius Spherical Inclusions

When it comes to poly-dispersed radius some parameters that were constant with the packing fraction in the monodispersed simulations becomes case-dependent. Fundamentally, we can show that the average chord length of the distribution is directly proportional to the second-order moment of the radius, which in this particular case can change depending on the values of the radius of the sphere randomly sampled. For this reason, with a fixed packing fraction and fixed mass, the results of the simulation are really variable. The parameters which can influence the dose equivalent rate measured are several, and also difficult to analyze: naturally the number of spheres of each realization can be very important, thus a bigger number implies smaller spheres, and thus a reduction of the self-shielding of the single source. It is also true that it is

possible to have geometrical interferences between a small sphere and a bigger one, placed between the direction that links the first one to the detector. It can be shown that, globally, the average of a big number of simulations converges towards the output results of the simulation with monodispersed radius spherical inclusion, if the radius used for this last one coincides with the maximum value of the poly-disperse case. The analysis was done simulating each time 1 gram of total mass with a density of $\rho = 6.6 g/cm^3$, for a packing fraction of $\xi = 0.00121$. To obtain a good accuracy, of about $PRSD \sim 0.25\%$ on average, 6000 batches of 5000 particles were required. Itis important to have a low standard deviation in this case, to give more importance to the discrepancy between different simulations. The results are shown in Figure 47.

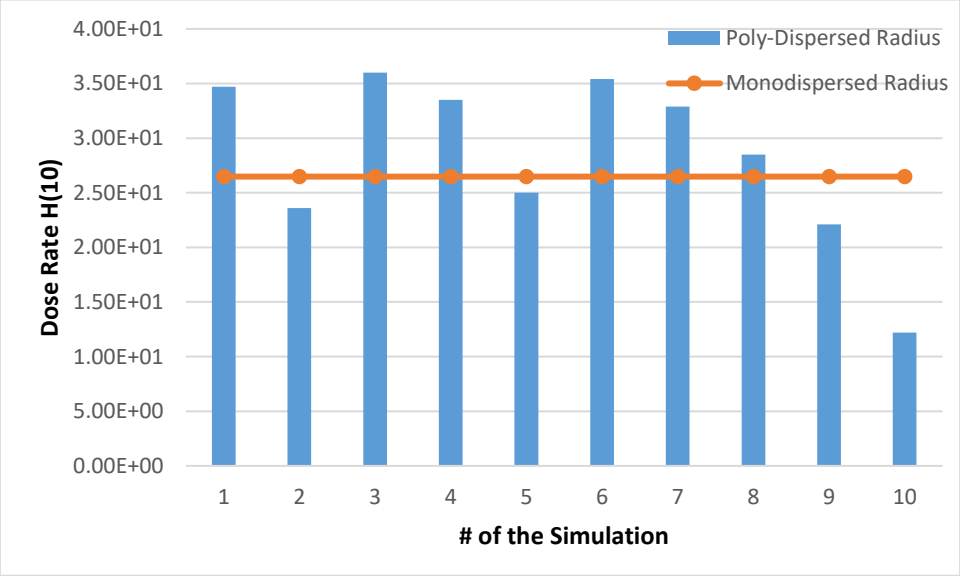

Figure 47: Comparison of different simulation results with Poly-dispersed radius spherical inclusions, at a fixed mass of 1 gram. Detection spot placed at 15 cm from the source. The Radii are sampled according to a uniform PDF. PRSD of the simulations ~0.25%.

In this simulation the values of the radius are homogeneously sampled between 1 millimeter and 10 micrometers, according to a uniform probability density function. The comparison with the homogeneous case is done using the results obtained with the simulation using the maximum radius of the Poly-dispersed ($1mm$).

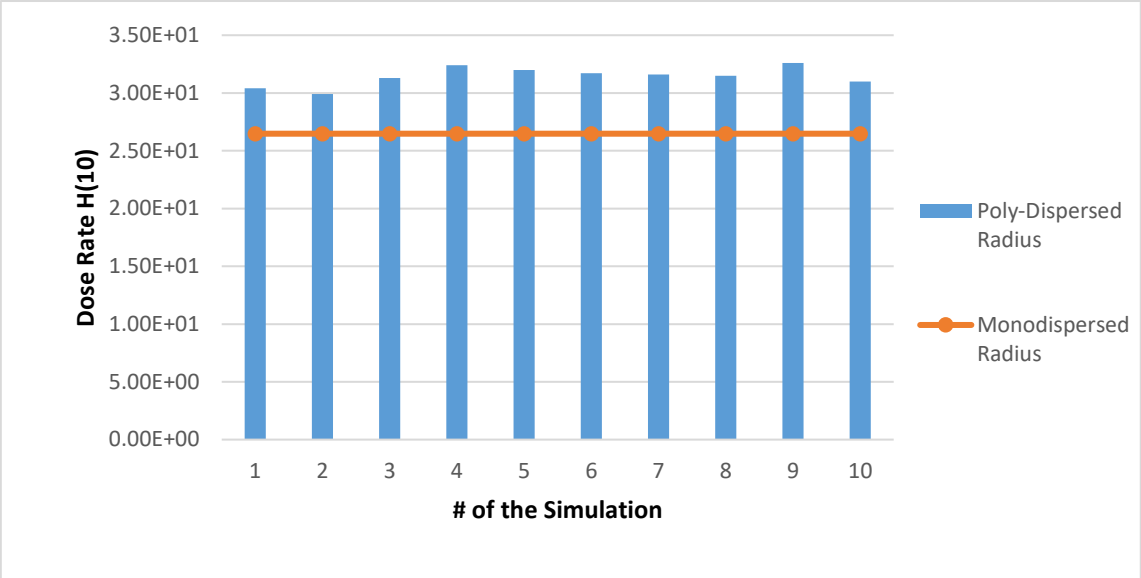

Figure 48: Comparison of different simulation results with Poly-dispersed radius spherical inclusions, at a fixed mass of 1 gram. Detection spot placed at 15 cm from the source. The Radii are sampled according to a log-normal PDF. PRSD of the simulations ∼0.25%.

Using the log-normal distribution instead of the uniform distribution, the dispersion between the radii decreases, since is more probable to have values close to the maximum ($1mm$). This leads also to a decreased dispersion in the output results, as shown in Figure 48. The parameters of the simulations were the same used in the previous case, with radii sampled from a uniform distribution.

Even if there are not important differences between the neutron simulations using poly and monodispersed radius inclusions, it is clear that the geometric disposition and the random sampling of the sphere diameter influences a lot the gamma dose detected.

4.7 Time Dependent Scenario

This analysis has again a different aim with respect to the cases described in 4.2, 4.3 and 4.5. The objective is not really understand the differences between the microscale and macroscale approach, but just to see if there are important differences between a steady-state scenario and a time-dependent one. Even if this is not the main issue of the topic, the results are reported for the sake of the completeness of the analysis. In fact, calculations with DARWIN-PEPIN 2® show that the ageing of the MOX in object leads to a great increase of gamma ray emission. Thus the dose equivalent rate curve we obtain doing the same analysis for the corner source done in section 4.2.1 is no more flat for great amount of mass, but it shows an increase of the slope, due to the increase of gamma emitter isotopes generated with the transitions of the MOX fuel. A comparison between the time dependent scenario and the steady state analysis (so the simple homogeneous model) is shown in Figure 49.

Each simulation is made using 100000 batches of 3000 particles for neutron calculations, for an accuracy of $PRSD < 1\%$, and 500000 batches of 5000 particles for gamma calculations, for an accuracy that goes from $PRSD \sim 0.25\%$ for the minimum amount of mass simulated to $PRSD \sim 0.65\%$ for the maximum one (as in the steady-state homogeneous case, the convergence is slower with high densities for gamma dose equivalent rates).

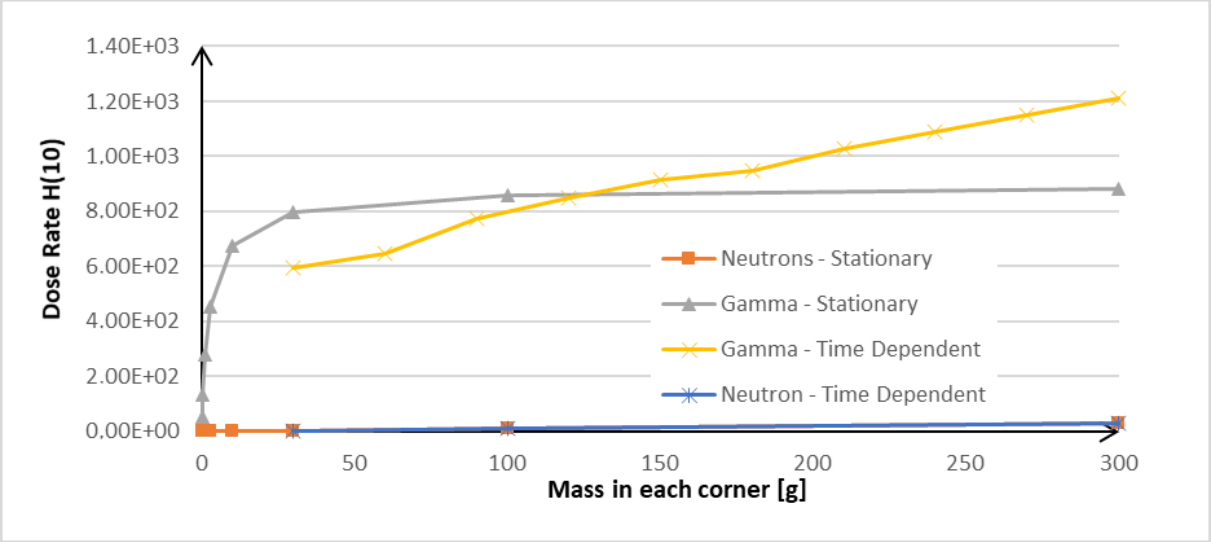

Figure 49: Comparison between dose rate calculated with the homogeneous model considering and without considering the evolution of the composition of the MOX during the time. PRSD < 0.7%.

The analysis involves a time range of 10 years. The calculation with the code DARWIN-PEPIN 2® for all the previous calculations was done taking into account an age of the MOX of 2 years, the time dependent analysis starts from an age of 1 year to arrive at 10. With the ageing of the source material the amount of gamma emitters increases, and this leads to a sensible increase of the source intensity for what concerns the gamma Photons. About the neutron dose, there are not changes in the results with respect to the previous simulation that can be comparable to the confidence interval of the simulations.

5 Conclusions

The parametrical analysis show that when it comes to particles with shorts mean free paths, such as gamma rays, dispersed and rarified sources are way more dangerous than a compact one. The effects of the self-shielding of the source is crucial, and depends a lot on density, disposition and dimension of the volumes. Naturally, in a fixed volume, these parameters are strongly correlated, and this leads to some collective effects. Having a really small dust grain diameter, or a really low density of this one leads to a drastic reduction of the absorption, with a consequent increase of the radioactive dose. The perfect dispersion is obtained homogenizing the properties, which leads to a packing fraction equal to 1, and we can assume that this case is the case where the dose is maximum. Thus the homogeneous model is, in the experiments examined before, always conservative, and it is particularly indicated to simulate geometries where the source is very rarefied. For example, a flat source like the one representing the dust on the Kyowa glass is well modeled by a situation of averaging of the properties. For situations in which the atomic mix limit is reached, like the neutron simulation in the same geometry, is trivial that there will be not differences between a homogenized model and a complex model, thus the homogeneous model is perfectly suitable also for this case. It is instead interesting studying how dust parameters affect the dose coming from gamma rays in compact sources using stochastic geometries. The parametrical analysis in object give us the possibility to understand that the dose rate is strictly correlated to the average chord length of the source geometry, and a shortening of this last one leads to a convergence with the maximum dose achievable, that is always the one coming from the homogeneous situation.

6 References

[1] D. Haas, A. Vandergheynst, J. Van Vliet, R. Lorenzelli and J. L. Nigon, Mixed-Oxide Fuel Fabrication Technology and Experience at the Belgonucléaire and CFCa Plants and Further Developments for the Melox Plant, *Nuclear Technology*, **106**, 1994, Pages: 77-81**.**

[2] A. Chetaine, R. Sanchez, L. Erradi, The use of the characteristics method to solve the transport equation in unstructured geometries, *Radiation Physics and Chemistry*, **61**(3–6), 2001, Pages: 763-765.

[3] C. Larmier, A. Zoia, F. Malvagi, E. Dumonteil, A. Mazzolo, Monte Carlo particle transport in random media: The effects of mixing statistics, *Journal of Quantitative Spectroscopy and Radiative Transfer*, **196**, 2017, Pages: 1-11.

[4] V. Rintala, H. Suikkanen, J. Leppänen, R. Kyrki-Rajamäki, Modeling of realistic pebble bed reactor geometries using the Serpent Monte Carlo code,
Annals of Nuclear Energy, **77**, 2015, Pages 223-230.

[5] M.M.R. Williams, E. W. Larsen, Neutron Transport in Spatially Random Media: Eigenvalue Problems, *Nuclear Science and Engineering,* **139** (1), 2001, Pages: 66-77.

[6] C. Larmier, *Stochastic Particle Transport in Disordered Media: beyond the Boltzmann Equation,* PHD Thesis, CEA Centre du Paris-Saclay, 2018, Pages: 9-18, 25-27.

[7] ICRP, The 2007 Recommendations of the International Commission on Radiological Protection. *ICRP Publication 103*, **37** (2-4), 2007, Pages: 61-78.

[8] Northwestern University, *Radiation Safety Handbook*, Office For Research Safety, Fargo, USA, 2010, Pages: 32.

[9] B. Davison, J. B. Sykes, *Neutron Transport Theory*, Oxford University Press, Oxford, UK, 1958, Pages: 15-27.

[10] M. Clark, K. F. Hansen, *Numerical Methods of Reactor Analysis*, Academic Press, New York, USA, 1964, Pages: 183-280.

[11] G.C. Pomraning, *Linear Kinetic Theory and Particle Transport in Stochastic Mixtures*, World Scientific Publishing, Los Angeles, USA, 1991, Pages: 55-83.

[12] W.J.M. de Kruijf, J.L. Kloosterman, On the average chord length in reactor physics, *Annals of Nuclear Energy*, **30**(5), 2003, Pages: 549-550.

[13] A. B. Davis, A. Marshak, Photon Propagation in Heterogeneous Optical Media with Spatial Correlations: Enhanced Mean-Free-Paths and Wider-Than-Exponential Free-Path Distributions, *Journal of Quantitative Spectroscopy and Radiative Transfer,* **84**(1), 2004 Pages: 3-34.

[14] I. Lux, L. Koblinger, *Monte Carlo Particle Transport Methods: Neutron and Photon Calculations*, CRC Press, Budapest, Hungary, 1991, Pages: 102-104.

[15] C. Robert, G. Casella, *Monte Carlo Statistical Methods*, Technometrics, New York, USA, 2000, Pages: 79-122.

[16] A. Zoia*,Simulation Monte Carlo pour le Transport de le Particules: notice theorique*, CEA Centre de Saclay, Saclay, France, 2018, Pages: 69-84.

[17] Web, https://atexmaterials.com/wp-content/uploads/2018/09/Lead-Acrylic.pdf

[18] G. Sengler, EPR Core Design, *Nuclear Engineering and Design*, **187,** 1999, Pages: 79-119.

[19] A. Tsilanizara, C. Diop, B. Nimal, M. Detoc, L. Luneville, M. Chiron, T. Huynh, I. Brésard, Eid, Mohamed , J. Klein, Roque, Bénédicte, P. Marimbeau, C. Garzenne, J. Parize, C. Vergne, DARWIN: An Evolution Code System for a Large Range of Applications, *Journal of Nuclear Science and Technology,* **37**, 2014.

[20] N.B. Garden, *Report on Glove Boxes and Containment Enclosures*, United States Atomic Energy Commission, Ann Arbor, USA, 1962, Pages: 75-85, 100.

[21] M.D. Dorrian, M. R. Bailey, Particle Size Distributions of Radioactive Aerosols Measured in Workplaces, *Radiation Protection Dosimetry*, **60**(2), 1995, Pages: 119-135

[22] K. Vishwa Prasad, Aereosol Size Distribution in a Uranium Processing and Fuel Fabrication Facility, *Radiation Protection Dosimetry,* **140**, 2010, Pages: 357-361.

[23] J. Shapiro, *Radiation Protection*, 4th edition, Harvard University Press, Boston, USA, 2002, Pages: 44-50.

[24] Ken B. Sorenson, *Safe and Secure Transport and Storage of Radioactive Materials*, Woodhead Publishing, Cambridge, UK, 2015, Pages: 123-140.

[25] J. Talbot, P. Scaaf, G. Tarjus, Random Sequential Addition of Hard Spheres, *Molecular Physics*, **72**, 1990.

[26] J. Ghassoun, A. Jehouani, Russian roulette efficiency in Monte Carlo resonant absorption calculations, *Applied Radiation and Isotopes*, **53**(4–5), 2000, Pages: 881-885.

[27] V. N. Manoharan, D. J. Pine, Building Materials by Packing Spheres. *MRS Bulletin*, **9**(2), 2004, Pages : 91-94.

[28] Sievert, Wikipedia, Web, https://en.wikipedia.org/wiki/Sievert.

[29] E. Mohamed, K. Khawla, F. Milad, Direct Mathematical Calculation of the Self-Shielding Factor for Cylindrical Radioactive Sources, *Journal of Taibah University for Science*, **10**(2), 2016, Pages: 266-270.

[30] K. H. J. Buschow, *Encyclopedia of Materials: Science and Technology,* Elsevier, New York, USA, 2001, Pages: 6377-6384.

[31] S. Torquato, *Random Heterogeneous Materials: Microstructure and Macroscopic Properties*, Springer-Verlag, Princeton, USA, 2013, Pages: 137-139, 166.